AFRL-PR-WP-TR-2006-2125

PULSE DETONATION PHYSIOCHEMICAL AND EXHAUST RELAXATION PROCESSES

Frederick R. Schauer, Ph.D.

Combustion Branch (AFRL/PRTC)
Turbine Engine Division
Propulsion Directorate
Air Force Materiel Command, Air Force Research Laboratory
Wright-Patterson Air Force Base, OH 45433-7251

MAY 2006

Final Report for 17 March 1997 – 12 May 2006

PROPULSION DIRECTORATE
AIR FORCE MATERIEL COMMAND
AIR FORCE RESEARCH LABORATORY
WRIGHT-PATTERSON AIR FORCE BASE, OH 45433-7251

NOTICE AND SIGNATURE PAGE

Using Government drawings, specifications, or other data included in this document for any purpose other than Government procurement does not in any way obligate the U.S. Government. The fact that the Government formulated or supplied the drawings, specifications, or other data does not license the holder or any other person or corporation; or convey any rights or permission to manufacture, use, or sell any patented invention that may relate to them.

This report was cleared for public release by the Air Force Research Laboratory Wright Site (AFRL/WS) Public Affairs Office and is available to the general public, including foreign nationals. Copies may be obtained from the Defense Technical Information Center (DTIC) (http://www.dtic.mil).

AFRL-PR-WP-TR-2006-2125 HAS BEEN REVIEWED AND IS APPROVED FOR PUBLICATION IN ACCORDANCE WITH ASSIGNED DISTRIBUTION STATEMENT.

*//Signature//

FREDERICK R. SCHAUER, Ph.D.
Project Monitor
Combustion Branch

//Signature//

ROBERT D. HANCOCK, Ph.D.
Chief
Combustion Branch

//Signature//

JEFFREY M. STRICKER
Chief Engineer
Turbine Engine Division
Propulsion Directorate

This report is published in the interest of scientific and technical information exchange, and its publication does not constitute the Government's approval or disapproval of its ideas or findings.

*Disseminated copies will show "//Signature//" stamped or typed above the signature blocks.

REPORT DOCUMENTATION PAGE

Form Approved
OMB No. 0704-0188

1. REPORT DATE *(DD-MM-YY)*	2. REPORT TYPE	3. DATES COVERED *(From - To)*
May 2006	Final	03/17/1997 – 05/12/2006

4. TITLE AND SUBTITLE
PULSE DETONATION PHYSIOCHEMICAL AND EXHAUST RELAXATION PROCESSES

5a. CONTRACT NUMBER
In-house

5b. GRANT NUMBER

5c. PROGRAM ELEMENT NUMBER
61102F

6. AUTHOR(S)
Frederick R. Schauer, Ph.D.

5d. PROJECT NUMBER
2308

5e. TASK NUMBER
P7

5f. WORK UNIT NUMBER
03

7. PERFORMING ORGANIZATION NAME(S) AND ADDRESS(ES)

Combustion Branch (AFRL/PRTC)
Turbine Engine Division
Propulsion Directorate
Air Force Materiel Command, Air Force Research Laboratory
Wright-Patterson Air Force Base, OH 45433-7251

8. PERFORMING ORGANIZATION REPORT NUMBER
AFRL-PR-WP-TR-2006-2125

9. SPONSORING/MONITORING AGENCY NAME(S) AND ADDRESS(ES)

Propulsion Directorate
Air Force Research Laboratory
Air Force Materiel Command
Wright-Patterson AFB, OH 45433-7251

10. SPONSORING/MONITORING AGENCY ACRONYM(S)
AFRL-PR-WP

11. SPONSORING/MONITORING AGENCY REPORT NUMBER(S)
AFRL-PR-WP-TR-2006-2125

12. DISTRIBUTION/AVAILABILITY STATEMENT
Approved for public release; distribution is unlimited.

13. SUPPLEMENTARY NOTES
Report contains color.

PAO case number: AFRL/WS 06-0270; Date cleared: 02 Feb 2006.

14. ABSTRACT
The objective of this program is to establish the scientific knowledge of detonation initiation, propagation, and blow-down needed to develop a pulse detonation engine (PDE) that will function on hydrocarbon fuels. The complex interaction of chemistry, gas dynamics, turbulent mixing, and geometry are responsible for the success or failure of the detonation phenomena required to operate a PDE. Detonation tube exhaust blow-down conditions, which are predicted to have a significant impact upon performance, will be explored in order to achieve basic understanding of the relationships between detonation, nozzles, and multiple detonation tube interactions.

15. SUBJECT TERMS
pulse detonation engine, plasma, detonation, Fischer-Tropsch (JP-8), detonation initiation, supercritical, ejector, pulsejet

16. SECURITY CLASSIFICATION OF:			17. LIMITATION OF ABSTRACT:	18. NUMBER OF PAGES	19a. NAME OF RESPONSIBLE PERSON (Monitor)
a. REPORT	b. ABSTRACT	c. THIS PAGE			Frederick R. Schauer, Ph.D.
Unclassified	Unclassified	Unclassified	SAR	48	19b. TELEPHONE NUMBER *(Include Area Code)* N/A

Standard Form 298 (Rev. 8-98)
Prescribed by ANSI Std. Z39-18

Pulse Detonation Physiochemical and Exhaust Relaxation Processes

LRIR 01PR02COR

Principal Investigator: Dr. Fred Schauer (AFRL/PRTC)

AFRL/PRTC
1790 Loop Road North, Building 490
Wright-Patterson AFB OH 45433-7103

SUMMARY/OVERVIEW:

The objective of this program is to establish the scientific knowledge of detonation initiation, propagation, and blow-down needed to develop a pulse detonation engine (PDE) that will function on hydrocarbon fuels. The complex interaction of chemistry, gas dynamics, turbulent mixing, and geometry are responsible for the success or failure of the detonation phenomena required to operate a PDE. Detonation tube exhaust blow-down conditions, which are predicted to have a significant impact upon performance, will be explored in order to achieve basic understanding of the relationships between detonations, nozzles, and multiple detonation tube interactions.

TECHNICAL DISCUSSION

The technological motivation for this program is the need to develop low-cost high-performance PDE's that can operate on hydrocarbon fuels. PDE's rely upon detonation combustion to produce a pressure rise in the combustion chamber instead of the expensive rotating machinery used in gas turbine engines. Consequently, the most expensive and maintenance-intensive components of a conventional turbine engine, namely the compressor and turbine stages, will not be necessary in PDE's. PDE's operates on a near-constant-volume heat addition cycle as opposed to the constant-pressure cycle employed in nearly all conventional aero-propulsion systems. The constant volume cycle offers improvements to specific thrust, specific fuel consumption, and specific impulse at a greatly reduced cost. In theory, the PDE can efficiently operate at Mach numbers from zero to above four without using

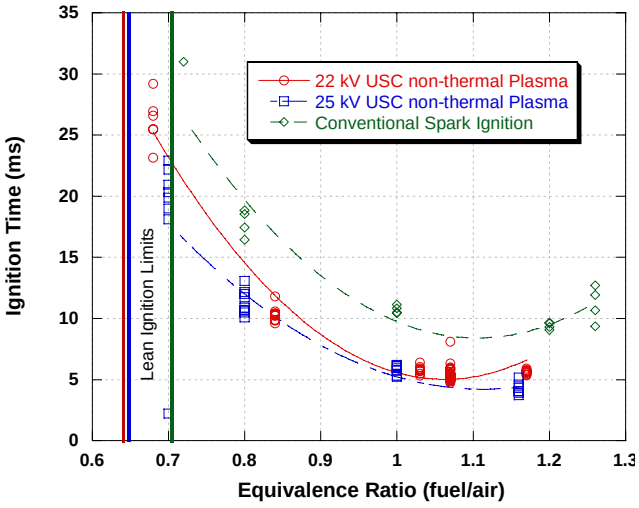

Figure 1. Non-thermal plasma ignition versus conventional spark ignition in a research PDE.

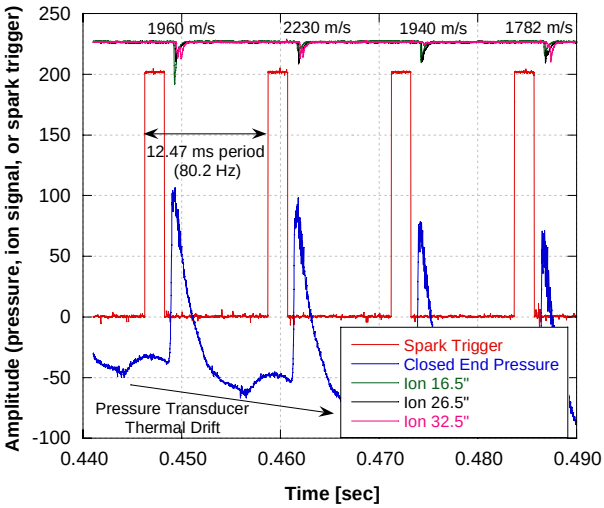

Figure 2. Hi-frequency detonation initiation in air.

a combined cycle/rocket approach. However, there are some major technical problems that must be resolved before the full potential of PDE's can be realized.

Foremost among the hurdles for a practical PDE system are the requirements for initiation and successful propagation of a detonation with hydrocarbon fuels in air. Although this has not been achieved in 60 years of PDE research, modern computational fluid mechanics (CFD), laser diagnostics, and high-speed instrumentation have not been applied to this challenge until recently. CFD and experimental studies of deflagration-to-detonation transition (DDT) and propagation are being carried out in order to explore the parameters controlling detonation initiation including: geometry effects, plasma ignition, hybrid fueled pre-detonators, and endothermic fuels.

Initiation time has previously been identified as a critical parameter for successful operation of a PDE. The majority of initiation time is chemical ignition time (from spark discharge to flame propagation). A novel method for reducing ignition time using a non-thermal plasma (or corona) ignition system has been under development. In collaboration with Prof. Martin Gunderson (USC) and Prof. John Yu (OSU), the non-thermal plasma scheme was compared to conventional spark ignition. Preliminary results, shown in Figure 1, indicate a significant reduction ignition time. However these results were not as low as those obtained at the Naval Post Graduate School in a valveless PDE. It is believed that the fill dynamics have an important role on initiation, producing turbulence and pressure gradients critical for initiation.

The fill dynamic affects become clear during high frequency operation, such as that shown in Figure 2, where prior to the detonation, high fill pressures are observed. Note the high thermal drift induced in the pressure measurements by heat flux due to the increased operating frequency. Flow dynamics from the high velocity fill process result in initial pressures well above the exit conditions. As shown here, if short initiation times can be obtained pressure losses from the expansion wave resultant from the valve closing can be avoided. However, initiation time becomes extremely critical, as the initial pressure drops well below ambient within typical hydrocarbon/air initiation times. The impact of valved versus valveless operation is a result of the complex interaction of turbulence, viscosity, chemistry, wall effects and gas dynamics.

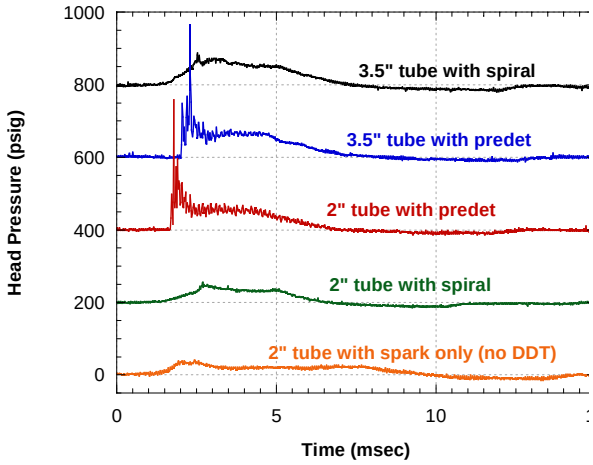

Figure 3. Head pressure versus time for various initiation methods.

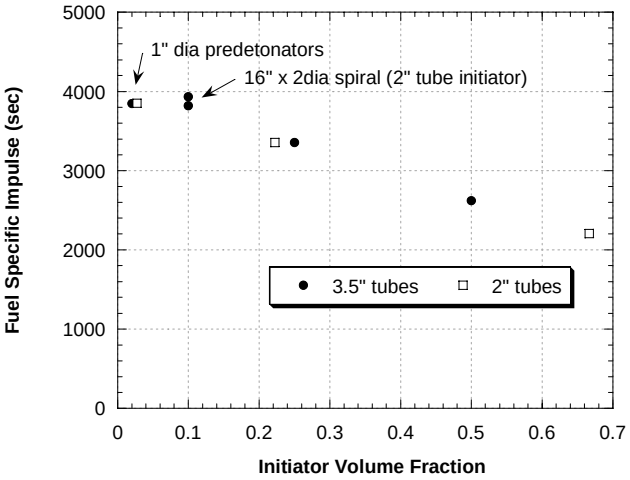

Figure 4. Specific impulse (fuel based) versus initiator volume fraction.

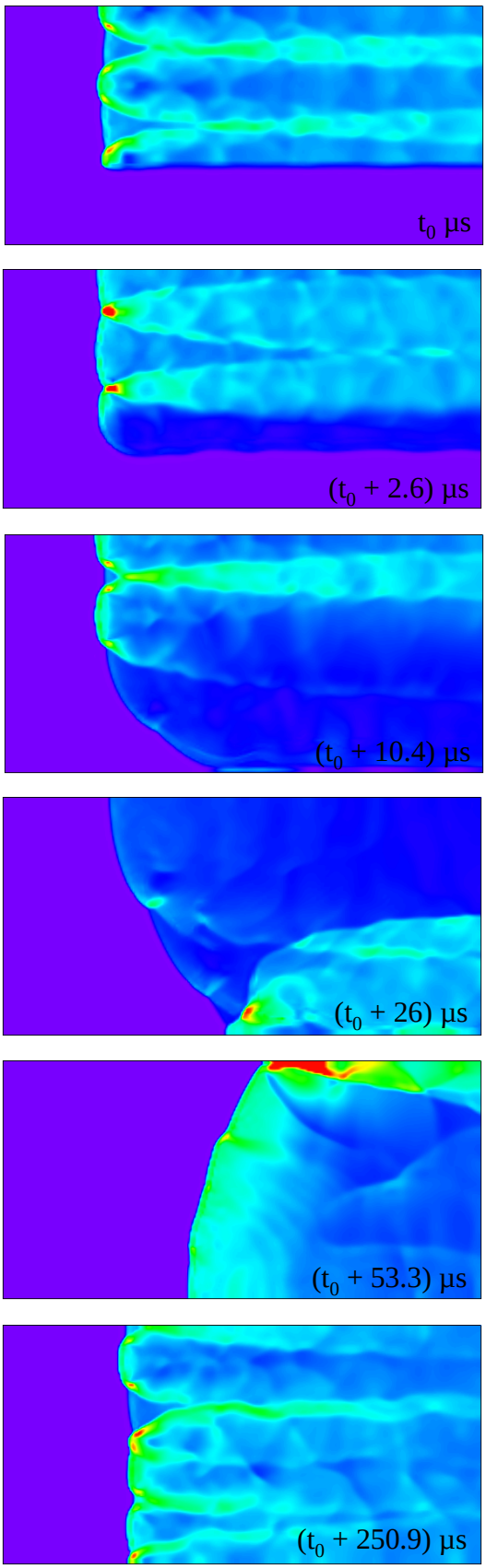

Figure 5. CFD of detonation transmission across sudden expansion.

Previously, identification of loss mechanisms which arise during the DDT process were quantified. For example, spiral losses have little impact upon exhaust relaxation times but attenuate thrust by as much as 40% due to supersonic drag during DDT and blowdown. Low loss initiation methods have been successfully developed and the impact is shown in Figures 3 and 4. By minimizing the inefficient initiation process to a smaller volume, initiation times and efficiency are both improved. As shown in Fig. 4, good efficiency can be achieved with reasonable initiation volumes. The key to this performance is efficient transmission of detonation from the small initiation volume to the thrust tube. CFD (such as that shown in Figure 5) and experimental work demonstrated that detonation transmission limitations can be circumvented by taking advantage of transverse wave reflections to nearly immediately re-initiate a quenched detonation propagating across an expansion. The same physics apply to the previously demonstrated split detonation initiation technique and will be applied to propagating a detonation continuously from tube-to-tube with nearly no loss due to imitation.

Due to the difficulty associated with obtaining detonations in air, it was previously thought that any fuel/air mixture which detonated must be well mixed. However, unaccounted losses in a detonating engine eventually were revealed to be poor mixing that still resulted in DDT. A 20% reduction in thrust can be observed due to the poor coupling of heat release and shock pressure rise, resulting in the reduced P_3 or thrust pressure levels shown in Figure 2 for the inhomogeneous case.

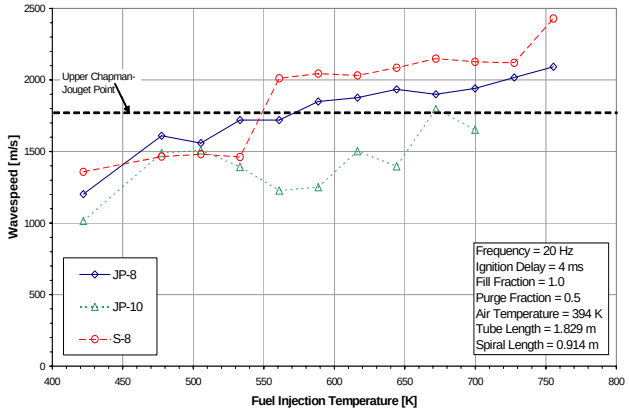

Figure 6. Detonation of standard military jet fuels compared to Fischer-Tropsch Fuel (S-8). using regenerative fuel cooled injection system.

Promising results from regenerative fuel cooling to provide supercritical fuel injection have been extended from 900F to 1100F. This system was used to take a preliminary look at the detonability of alternative military fuels, such as coal-derived Fischer-Tropsch, with results shown in Figure 6. A catalyst is being applied to the next-generation, higher temperature heat exchanger in order to promote endothermic effects which will theoretically promote DDT.

Progress in exhaust relaxation processes includes nozzle studies, back pressurization at altitude, and unsteady detonation/ejector flow dynamics. The unsteady detonation blow down process is conducive to exhaust vortex formation, which interacts with ejector inlets for dramatic performance improvements. Scaling results

Progress in exhaust relaxation processes includes nozzle studies, back pressurization at altitude, and unsteady detonation/ejector flow dynamics. The previously identified, unsteady detonation blow down process is conducive to exhaust vortex formation, which interacts with ejector inlets for dramatic performance improvements. Results were obtained for various sizes and exit conditions, such as those shown in Figures 7 and 8. In general scaling rules were found to be consistent despite the variation of parameters when scaled by vortex formation dimensions as shown in Figure 9 for a range of unsteady ejectors. These results are consistent with previous results: as the formation number goes to zero, the driver becomes steady and peak augmentation ratios become ~20%, as confirmed by conventional ejector results. The dynamic vortex formation from a pulsed detonation event can produce twice the augmentation.

Further detail on detonation initiation, fuel preparation, and thrust augmentation is provided in the following sections entitled Impact of Detonation Initiation Techniques on Thrust in a Pulsed Detonation Engine, Cycle Performance of a Pulse Detonation Engine with Supercritical Fuel Injection, and Performance Scaling of a Large Scale Unsteady-Driven Ejector System, respectively.

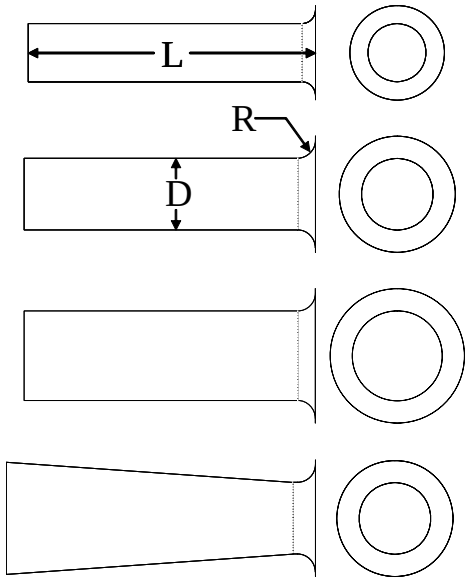

Figure 7. Representative ejector schematics and symbols for relevant dimensions for straight walled and tapered ejectors evaluated.

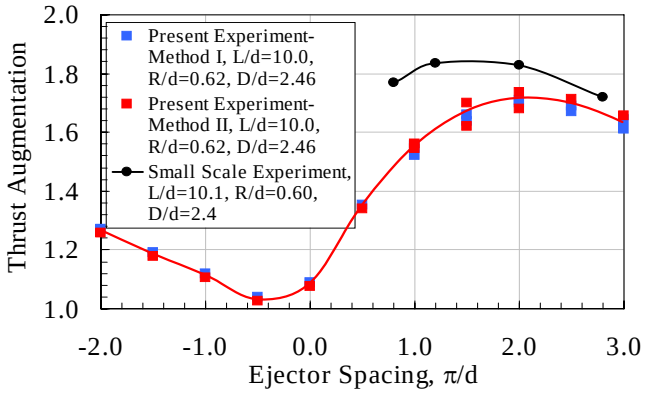

Figure 8. Thrust augmentation as a function of driver-to-ejector spacing for the D/d=2.46, L/d=10.0 ejector.

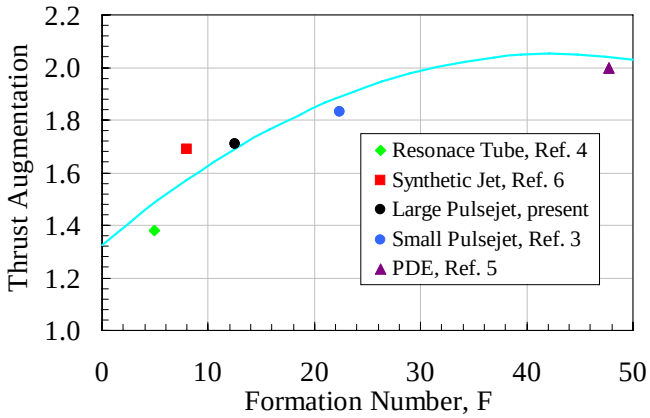

Figure 9. Peak thrust augmentation as a function of Formation Number for unsteady ejectors, see AIAA 2006-4216 for further details

Impact of Detonation Initiation Techniques on Thrust in a Pulsed Detonation Engine

Detonation initiation remains an impediment to pulsed detonation technology efficacy. Practical fuels can now be detonated regularly in the laboratory using conventional oxygen-rich predetonators or extended deflagration-to-detonation transition (DDT) geometries; however, these systems are not suited for field use due to the excess oxygen required for the predetonator and the reduced performance due to drag of DDT mechanisms. The performance of a hydrogen-air multi-cycle pulsed detonation engine is examined using two initiation schemes, a predetonator and a DDT device to determine a suitable initiation mechanism. DDT mechanisms typical for initiation of hydrogen and those typical of insensitive hydrocarbon fuels are examined. Because of the relative ease of detonation initiation, hydrogen is the fuel used in the main detonator tube, even with the longer DDT mechanisms used for insensitive fuels. The predetonator uses aviation gasoline and nitrous oxide in a small (1 to 3% of the volume of the main tube) chamber to initiate a detonation and generate an upper limit on the expected performance of DDT initiators. A fuel-specific impulse value of approximately 3900 sec is achieved with the predetonator at 10 Hz and an equivalence ratio and fill fraction of unity. For DDT initiation, a Schelkin-like spiral located in 10 to 70% of the main detonation tube volume is used. Below 10% of the main tube volume, DDT is found to generate identical impulse to the predetonator initiation, while for the longest DDT mechanism, located throughout 70% of the main tube volume, a reduction in fuel-specific impulse of 44% is measured. Head pressure measurements show a reduced thrust wall pressure for the DDT initiation, probably owing to the drag and dissipation of the retonation wave traveling upstream through the DDT mechanism.

I. Introduction

PULSED detonation engines (PDEs) require efficient detonation initiation for practical operation. Typically detonation initiation is obtained via the use of predetonators, which utilize a more readily detonable mixture in a small initiation tube that subsequently propagates a detonation into a main thrust detonation tube, and/or flame acceleration through successful deflagration-to-deflagration transition (DDT)[1]. Depending on the sensitivity of the fuel, the amount of excess oxygen or DDT distance can become excessive. In recent years, kerosene-air mixtures have been detonated successfully in a variety of engine scale detonation tubes[2-5]; however, the practicality of the methods used to achieve hydrocarbon detonations continues to be an obstacle to PDE development.

Although predetonators can produce extremely short detonation initiation times and distances, they typically employ highly reactive components to overcome the difficulties associated with hydrocarbon-air detonation initiation. In addition to the logistic and hardware penalties associated with typical predetonator systems, minimizing the required size and obtaining efficient transition to a practical hydrocarbon-air mixture remain challenges. Typically oxygen is utilized due to its high reactivity and nominal detonation initiation requirements with hydrocarbon fuels. Oxygen is unpleasant to work with due to its proclivity for exothermically oxidizing structural components. Additionally, even a 2% by-volume predetonator requires a significant oxygen supply.

DDT has been demonstrated successfully in hydrocarbon-air mixtures. Although high-energy ignition system or excess oxidizer may not be required, DDT typically requires both long distances and times for practical hydrocarbon-air mixtures. Significant cycle time penalties and inefficiencies have been identified as the negative consequences of hydrocarbon-air DDT used for the initiation process[6]. Most hydrocarbon-air mixtures can be readily detonated with a 48″ Schelkin spiral if good mixing can be obtained[5]. However, the performance penalties for using long spirals can be quite significant. Kailasanath's review found that the generally recognized fuel based specific impulse for hydrogen air mixtures is around 4000-4500 seconds (with a fully detonating tube)[7].

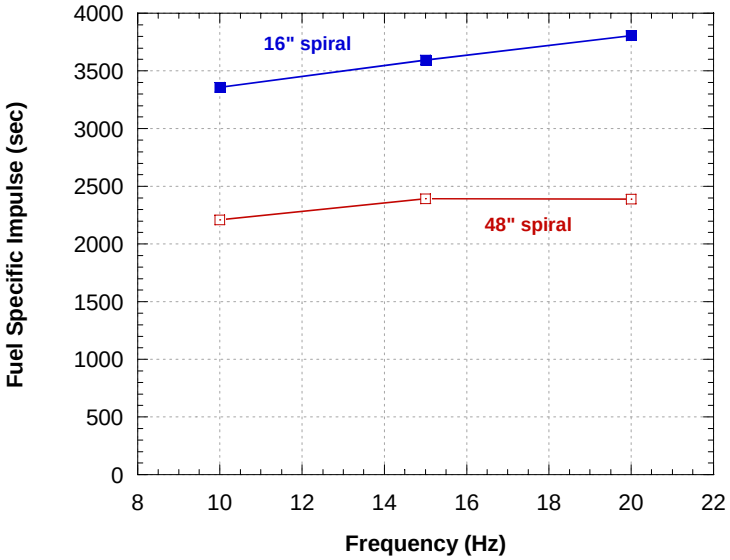

Figure 1. Specific impulse versus frequency for stoichiometric hydrogen-air with 16″ and 48″ spirals in a 72″ long, 2″ diameter tube.

Our past work[6] demonstrated that even a 16″ spiral in a 72″ tube has an I_{sp} below 4000 seconds, and as shown in Fig. 1, the performance penalties associated with a long spiral are nearly 50%. These penalties were found to be caused by DDT obstacle drag in the blow-down processes and are in addition to pressure drop penalties which occur during the tube fill cycle. The authors found that turbulence and pressure effects can promote detonation initiation and enhance performance as shown by the I_{sp} increasing with frequency with a 16″ spiral. However, losses offset gains when longer spirals are utilized, such as the 48″ Schelkin spiral, (the performance of which is shown in Fig. 1.) which may be required for initiation of conventional hydrocarbon-air mixtures[5].

Shepherd and co-workers found similar penalties associated with DDT processes in their detonation impulse measurements[8]. This paper will further quantify the performance of DDT initiation and transmission mechanisms in comparison to predetonators.

II. Experimental Setup & Procedures

Experiments were conducted using the research PDE at the Air Force Research Laboratory's Pulsed Detonation Research Facility. This PDE uses the "head" of a General Motors automotive engine to control the airflow into the detonation tube. The PDE cycle consisted of equal time allotted for: i) filling the detonation tube with pre-mixed hydrogen and air at an equivalence ratio of one, ii) ignition, detonation, and blow-down, and iii) purging of the detonation tube with air. For these experiments the pressure upstream of the automotive poppet valves was controlled such that during the fill cycle the mass flow of pre-mixed fuel and air was equivalent to the volume of the tube times the density of the fuel-air charge at the gas temperature upstream of the poppet valves and atmospheric pressure times the operating frequency. This was defined as a fill fraction (FF) of one, and all tests during this research were conducted at a fill fraction of one unless otherwise noted. The purge fraction (PF) was defined in the same manner and was held constant at one-half for all experiments. The fuel-air mixture was ignited with a 115 mJ spark at the closed end of the main tube or predetonator. Further details of this engine are given by Schauer et al[9].

The PDE was operated at 10Hz in order to minimize turbulent and dynamic pressure effects on the initiation processes and PDE performance. Unless otherwise noted, a stoichiometric mixture of hydrogen-air was used in the main detonation tube (equivalence ratio of unity). Detonation tubes were instrumented with a dynamic pressure transducer at the closed end of the tube and ion probes at various intervals along the length of the detonation tube. Thrust was measured on a damped thrust stand where displacement was proportional to thrust. The thrust stand was oscillated during each test, and the displacement averaged over several seconds to eliminate hysteresis and improve accuracy. The repeatability of the thrust measurement has been shown previously to be within ±2%[6].

Figure 2. 16″ long x 2″ diameter initiation section with Schelkin-type spiral connected to a 3.5″ diameter detonation tube. Additional details of the 2″ initiation section and ~17° half-angle transmission section are shown on the right.

For the purposes of assessing initiation on performance, two tube diameters were chosen and two initiation mechanisms were employed. A 2″ diameter, 16″ long Schelkin-type spiral was located in the head end of a 16″ long 2″ diameter pipe which was then connected to either more 2″ diameter pipe (as described in previous work and in Fig 3a.), or through a ~17° half-angle coupling (2″ to 4″ pipe reducer fitting) to a 3.5″ diameter pipe as shown in Fig. 2 and 3b. The initiation section was approximately 10 and 20% of the tube volume of the 3.5″ and 2″ main tubes respectively.

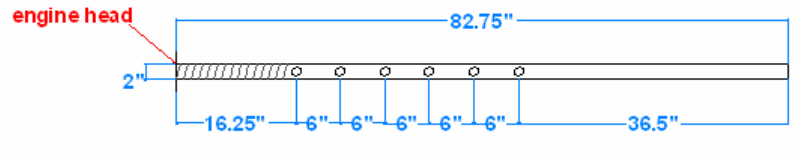

a). 2″ tube with spiral

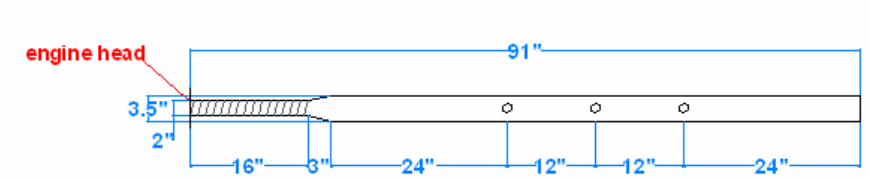

b). 3.5″ tube with spiral

Figure 3. Geometry and instrumentation locations of 2″ (a) and 3.5″ (b) diameter detonation tubes, each initiated via a 2″ diameter x 16″ long Schelkin-type spiral section located adjacent to the closed ignition end.

An avgas-nitrous oxide predetonator was the second initiation scheme. The predetonator, pictured in Fig. 4, consisted of an outboard marine company's (OMC) two-stage injector originally developed for 2-stroke direct injection applications as well as an automotive company's high pressure direct injection injector. In this application, the fuel was injected at approximately 120 psig by the OMC injector and liquid nitrous oxide was injected by the high pressure direct injector at 600 to 800 psig, (dependant on the bottle supply temperature.) The second stage of the OMC injector was used to purge the predetonator at the end of a cycle with compressed air at 95 psig. The injectors were attached to a 1″ pipe cap that screwed onto a 1″ tube attached to an adapter. In this manner, the detonation was transferred from the predetonator to the main detonation tube.

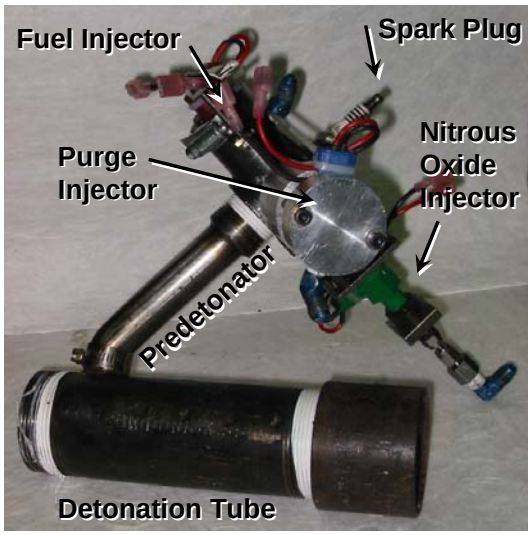

Figure 4. Avgas-nitrous oxide predetonator consisting of three fuel injectors, 1″ tubing and a spark plug.

The predetonator transmitted the resultant detonation to either a 2″ or 3.5″ diameter main detonation tube containing a hydrogen-air mixture supplied by the research engine head. The transmission section was carefully designed to propagate the detonation from the predetonator to the main tube without quenching. Hardware configuration and instrumentation ports for the predetonator initiated hardware are shown in Fig. 5.

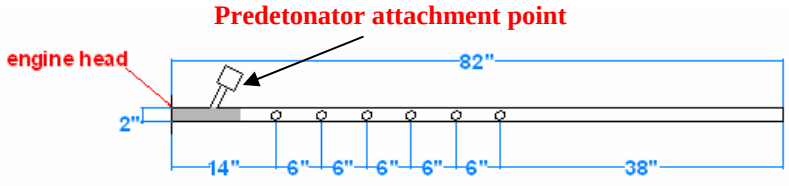

a). 2″ tube with predetonator

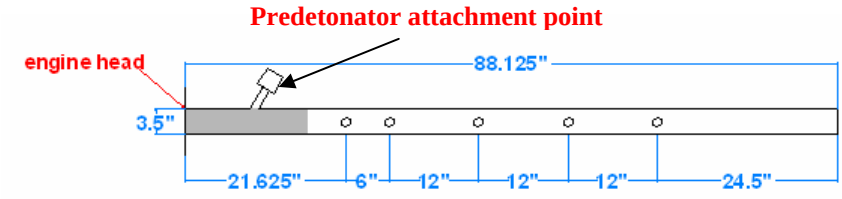

b). 3.5″ tube with predetonator

Figure 5. Geometry and instrumentation locations of 2″ (a) and 3.5″ (b) diameter detonation tubes, each initiated via a 1″ diameter predetonator near the head end.

The predetonator was found to operate reliably with either vapor or liquid fuels, although liquid avgas was used here. Nitrous oxide was found to have the detonability of pure oxygen, but without the special handling and design requirements associated with pure oxygen. The use of liquid nitrous oxide was also beneficial because of the cooling from the heat of vaporization upon injection, which kept the injector assembly cool as shown in Fig. 6. The 1″ diameter predetonator produced a detonation consistently within 6″. Consequently a 7″ long predetonator was employed, producing a predetonator volume ~1-3% of the main detonation tubes.

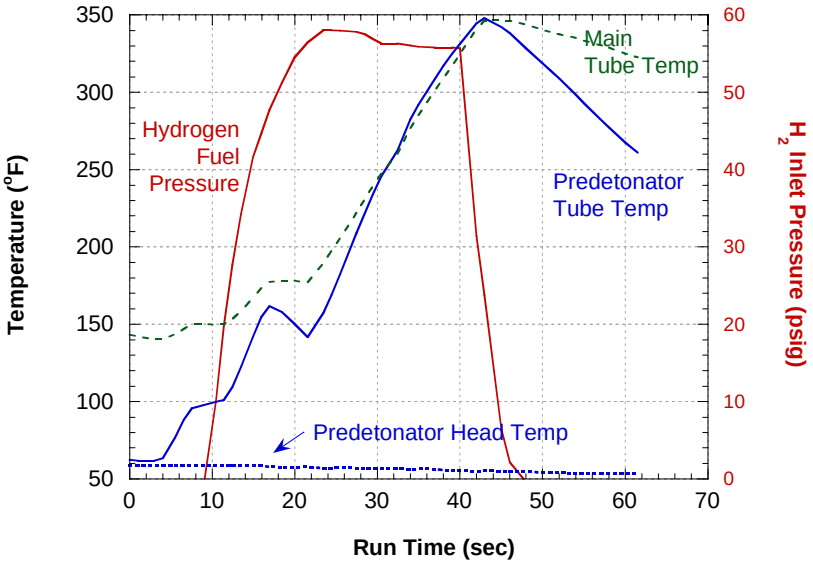

Figure 6. Temperature of predetonator head, predetonator combustion tube, and main thrust tube versus run time. H_2 pressure plotted for reference. Data acquired between 30 and 40 seconds.

In order to obtain consistent blow-down dynamics, all four geometries described were within 10% of the same length. Subsequently the four geometries will be referenced by main tube diameter and initiation method, e.g. "3.5″ tube with spiral" refers to the geometry shown in Fig. 3b., "2″ tube with predetonator" corresponds to the geometry shown in Fig. 5a., etc.

Operation consisted of setting frequency, main combustion air and purge air flow rates, followed by turning on the ignition system and/or predetonator. The main tube hydrogen fuel was then enabled and data collection commenced once the hydrogen fuel flow rate was stabilized. Consequently, the main detonation tube wall temperatures were ~300°F for all experiments. As typified in Fig. 6, data were collected between 30 and 40 seconds for the all experiments.

In some cases, the predetonator geometries were operated with a conventional spark in the main tube head with the predetonator off. As there was no geometry to aid DDT in these cases, no measurable detonation wavespeeds were observed. Consequently, these cases are subsequently referred to as "spark (no DDT)".

III. Experimental Results

With both the spiral and predetonator initiators, DDT was obtained for both tube diameters, as shown in Fig. 7. The limited measurements presented here demonstrate that stable detonation wavespeeds were obtained for all four cases. Additional measurements indicated that detonation was achieved within the spiral or predetonator (as appropriate) and successfully transferred down the main detonation tube.

Although no wavespeeds were observable with ion probes for the spark only case, dynamic head pressure and average thrust measurements indicated significant pressure was achieved despite the failure to achieve detonation. This is clear in Fig. 8, in which the dynamic head pressures are compared for the varying tube sizes and initiation methods. Head pressures are off-set 200psi for each case in the interest of intelligibility for Fig. 8, but will be compared in further detail below. Previous measurements of 'bare' tubes' with high speed pressure transducers indicated that the flame was nearly detonating at the end of the tube under similar conditions but did not transition according to the current instrumentation.

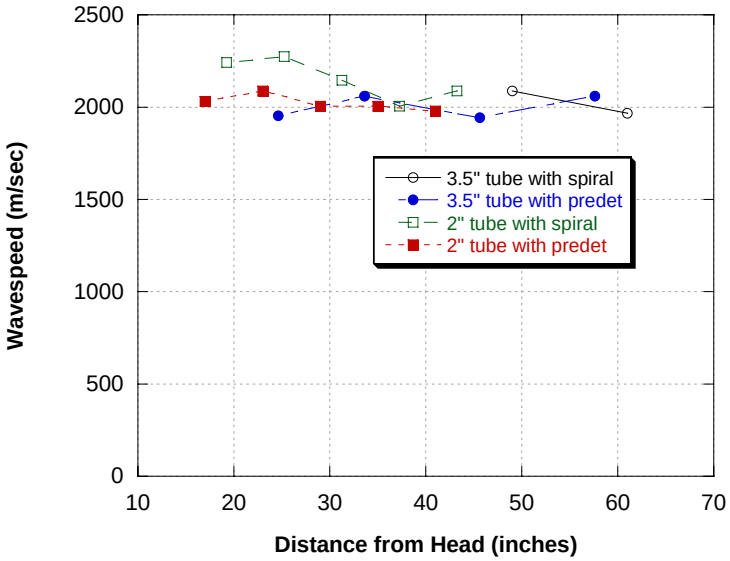

Figure 7. Ion probe wavespeed measurements confirming detonation initiation for the both tube diameters and initiation schemes. Note that the Chapman-Jouget wavespeed for stoichiometric hydrogen-air is 1970 m/sec[11].

For some cases, the head pressure could be integrated with time and area to provide a measure of pressure thrust[8], as shown in Fig. 9 for the 2″ tube with predetonator case. The average thrust was measured via the damped thrust stand. Before placing much significance on such thrust comparisons, it should be noted that the dynamic pressure transducers are noisy and sometimes experience significant thermal and DC drift. The integrated head pressure thrust measurement is highly sensitive to small DC offsets or changes in slope to the dynamic pressure signal.

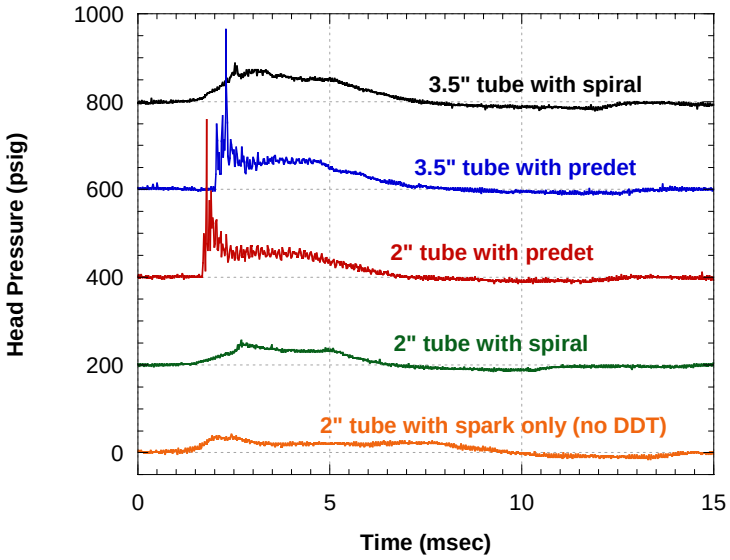

Figure 8. Head pressure traces versus time. Times are normalized to spark discharge and each pressure is offset 200psi for clarity.

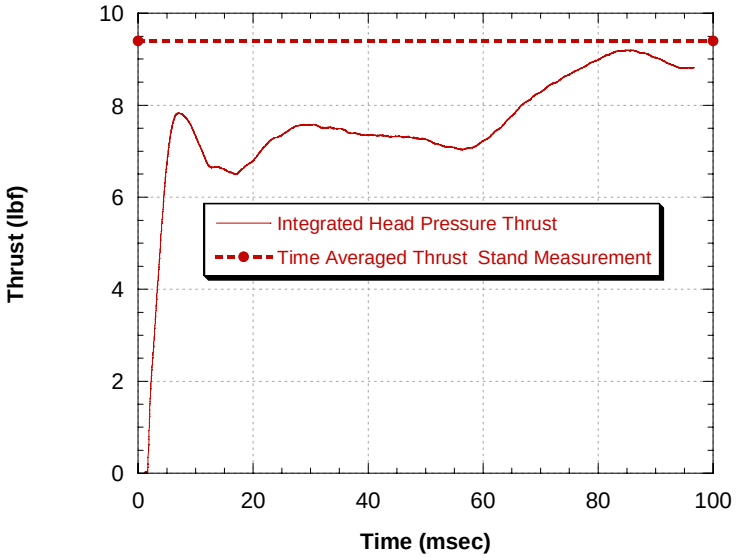

Figure 9. Integrated head pressure trace for one cycle in the 2″ tube with predetonator. The average thrust is also plotted for comparison purposes and was obtained via the damped thrust stand.

Test data is summarized in Table 1, which indicates: the total tube length, the blow-down time as measured from beginning of pressure rise to the zero crossing of blow-down pressure (gauge), the ignition time from spark discharge to the beginning of head pressure rise, the DDT time from 'ignition' pressure rise to the first ion probe, the air thrust, the air thrust plus predetonator thrust, thrust (total) as measured by the damped thrust stand, and the integrated head pressure indicates the integrated head pressure thrust as demonstrated in Fig 9. In several instances, 'na' indicates the relevant parameter is not applicable. As defined above, the ignition time poorly reflects the actual predetonator performance as pressure rise begins well before the head pressure transducer indicates. Integrated pressure thrust is calculated based upon an assumed area and as noted by Shepherd et al.[8], is not very accurate when obstructions such as spirals are present.

Table 1. Summary of test data.

Test Configuration and Data Summary	2″ tube with 16″ spiral	3.5″ tube with 16″x 2″ dia spiral	2″ tube with 1″ dia predet	2″ tube, spark (No DDT)	3.5″ tube with 1″ dia predet	units
Total Length	83	91	82	82	88	in
Blow-down Time	3.9	5.0	5.1	7.7	4.9	msec
Ignition Time	1.2	0.8	1.7	1.2	2.0	msec
DDT Time	1.5	1.7	0.1	na	0.3	msec
Air Thrust	1	3.8	1	0.9	3.8	lbf
Air + Predet Thrust	na	na	1.6	na	4.8	lbf
Thrust	6.4	25.7	9.4	5.8	30.8	lbf
Integrated Head Pressure	4.4	25.5	9.2	5.8	30.2	lbf

Using damped thrust stand measurements, a fuel-based specific impulse was calculated for the subsequent plots. For these calculations, the predetonator mass flux was neglected. It is debatable whether this is a good assumption, but as noted previously, the predetonator volumes were small (~2%) and similar results have been demonstrated via cross tube ignition without the predetonator fuel and oxidizer penalties[12].

The specific impulse was plotted versus initiator section volume fraction as shown in Fig. 10, included are several previously obtained results[6]. The initiator volume fraction is defined as the initiator section tube volume (either the entire spiral or predetonator section) divided by the total tube volume.

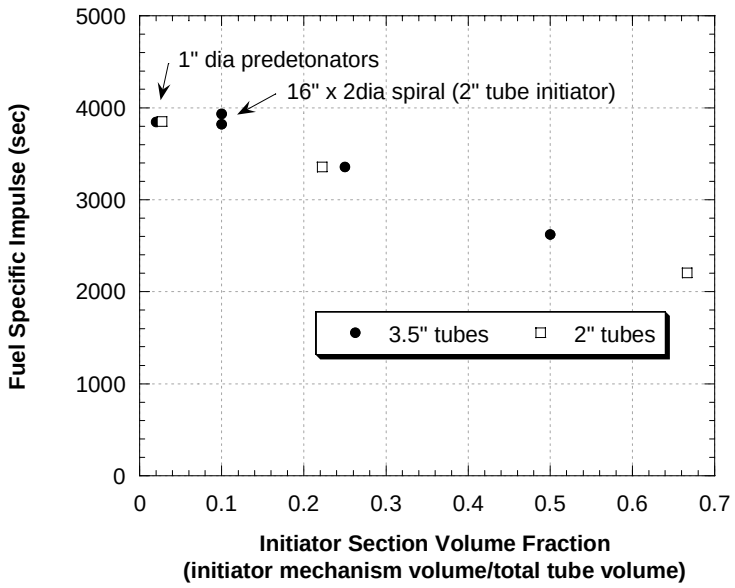

Figure 10. Specific impulse (fuel based and predetonator neglected) versus initiator volume fraction.

The above data enable an assessment of detonation initiation performance. Several additional parameters were varied in order to appraise performance sensitivity. Variations in equivalence ratio and fill fraction have dictated detonation performance results in the past; so these parameters were examined in the context of initiation performance.

Having varied equivalence ratio using spirals previously, the main tube stoichiometry was varied with the predetonator initiated schemes and compared to Shepherd's model[9,13]. Figure 11 illustrates, as before, that good agreement (within 10%) was obtained with Shepherd's predicted value of 4335.4 seconds at stoichiometric conditions. Conventional spiral initiated tubes had lower DDT limits of 0.6-0.8 equivalence ratio for 2″ tubes and 0.8-0.9 equivalence ratio for 3.5″ tubes. The sudden decreases in specific impulse show that the predetonator initiator improved only modestly at best upon these limits, but surprisingly, Chapman-Jouget detonations were observed intermittently at even the lowest equivalence ratios as shown by the open symbols.

Similarly, varying fill fraction with both the most efficient of the initiation schemes (3.5tube with spiral and predetonators) produced good agreement with Shepherds model[14] as shown in Fig. 12. The model was fit to an I_{sp} of 4000 sec at a fill fraction of one (fully detonating tube), which is about the best our group has been able to obtain experimentally with multi-cycle experiments. It should be noted that it is difficult to determine the exact fill fraction/local equivalence ratio during multi-cycle operation as previous experiments have shown that the fill process is far from slug-flow[15]. This is not to say that the fuel and air-flow rates through the engine were not precise, but rather that there was mixing between the purge air and the fuel-air charge of the next cycle as well as mixing of the fuel-air charge with ambient air at the end of the detonation tube. At the end of the detonation tube, the momentum of the in-flowing fuel-air charge carries it slightly past the exit of the detonation tube, creating a slight vacuum in the detonation tube (similar to the overexpansion that occurred after the blow-down process, but smaller in magnitude), which caused a mixture of fuel-air, purge air, ambient air and possibly exhaust to be pulled into the exit of the detonation tube in a spring-like action. The equivalence ratio in the last 12 to 18″ of the detonation tube is at-best unknown and the wave speed in this region typically deteriorates.

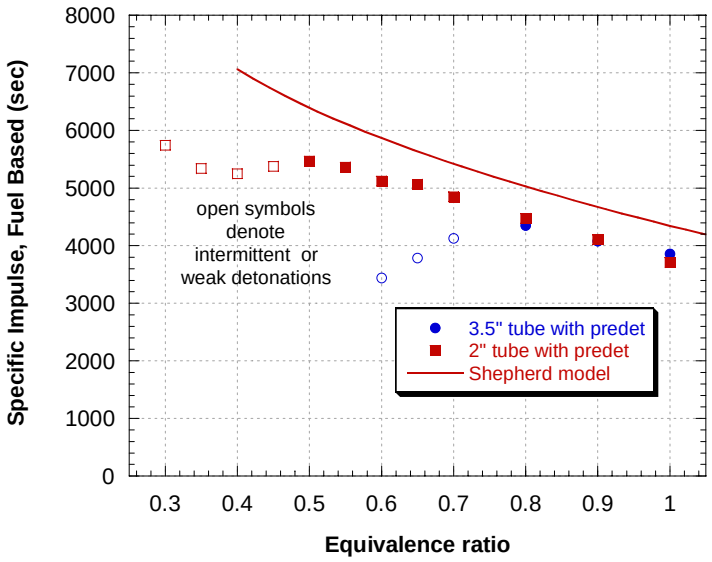

Figure 11. Specific impulse versus equivalence ratio for predetonator initiated tubes in comparison with Shepherd's model[9,13].

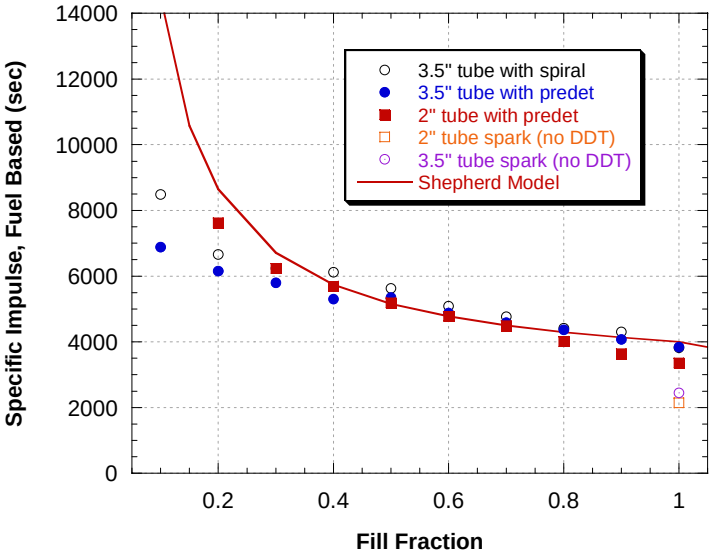

Figure 12. Specific impulse versus fill fraction (detonation reactant volume/total tube volume) in comparison with Shepherd's model[15].

IV. Performance Analysis & Discussion

From the head pressure traces of Fig. 8, it is clear that predetonator initiated detonations produced near direct initiation of the main detonation tubes, as evidenced by the near von Neuman pressure peaks obtained. The spiral initiated cases universally produced sub Chapman-Jouget head pressures and it appears that spiral drag significantly weakens the retonation wave in addition to attenuating pressure thrust, as confirmed by Shepherd[8]. The obstruction-weakened retonation wave is more clearly visible in Fig. 13. below, where head

pressure has been normalized to the blow down time for the three 2″ diameter tube cases. The spark with no DDT case clearly shows more thrust pressure than the spiral case in both Fig. 13 and Table 1. Yet the actual thrust measurement shows that it is better to have DDT even with the losses due to drag associated with the DDT mechanism (the spiral). Dynamic pressure transducer measurements in multi-cycle detonating environments are qualitative due to thermal and DC drift. Interestingly, the slow flame-speed results in a prolonged head pressure trace for the non-detonating case.

The integrated pressure method of calculating thrust is nearly meaningless for reasons cited above when spiral drag is significant, but is useful when there are no or minimal obstructions in the tube, such as the predetonator cases and the spark (no DDT) case shown in Table 1. By transitioning a 2″ diameter spiral initiated tube section to a larger tube, spiral drag losses were minimized and produced virtually identical performance as the near-direct initiation via predetonator method, as seen in Fig. 10. It should be noted that although the expansion angle of the transition from 2″ diameter to 3.5″ diameter is larger than typically acceptable for detonation diffraction without quenching[16], transverse wave reflections likely re-establish the detonation quickly for such a small area change[17].

Figure 10, clearly indicates a strong correlation between initiator volume and PDE performance. A nearly 50% reduction in efficiency occurs with increasing initiator volume. This decrease in efficiency at high initiator volumes is especially significant for difficult to detonate mixtures such as kerosene-air, as larger DDT volumes are required.

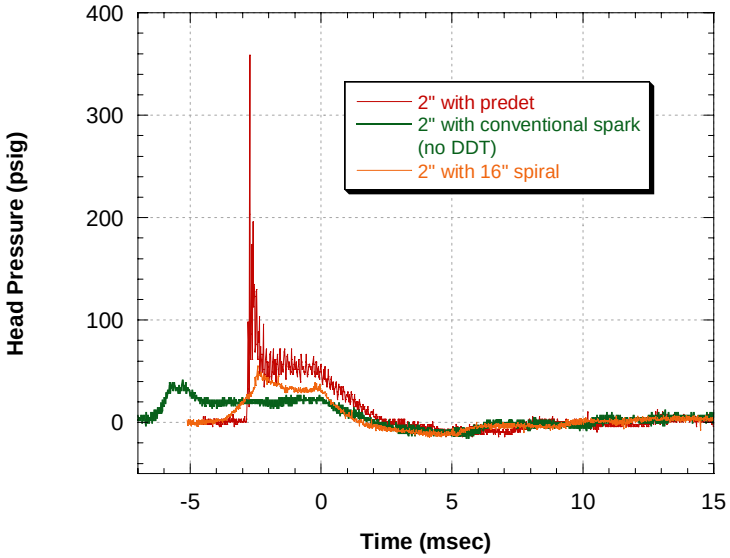

Figure 13. Head Pressure for 2″ diameter tube cases normalized to blow down.

The impact of initiation upon throttling performance (via fill fraction), becomes even clearer when larger spirals were added to the 3.5″ diameter detonation tube, producing the results shown in Fig. 14. Losses evident at full tube fill (the full throttle condition), continue to degrade efficiency when the fill fraction is reduced.

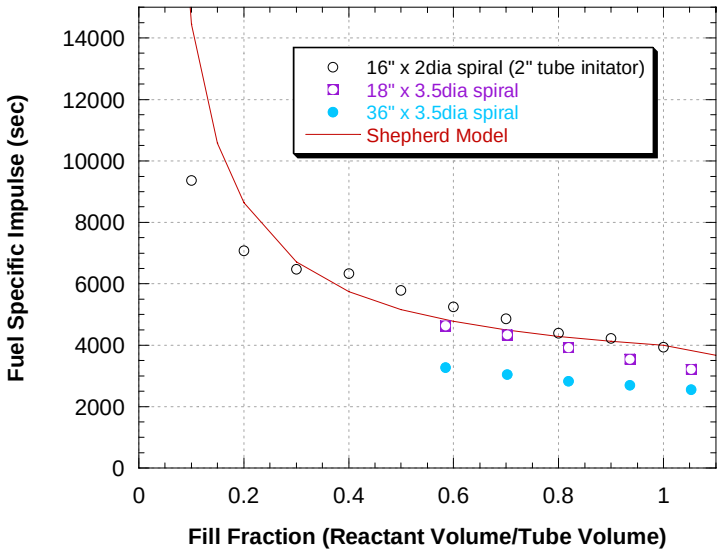

Figure 14. Specific impulse versus fill fraction (detonation reactant volume/total tube volume) in comparison with Shepherds model[14] for 3.5″ diameter tubes with varying 3.5″ diameter Schelkin-type spiral initiators.

V. Conclusion

Pulsed detonation engine performance was shown to be sensitive to initiation strategy, varying over 40%, with the best initiation strategies approaching predicted performance. Predetonator initiation was used to provide an upper bound of 3900 sec for DDT initiation strategies, as well as to compare with current models. The predetonation initiation scheme was within 15% of predicted fuel-specific impulse for equivalence ratios from 0.5 to 1 and fill fractions from 0.3 to 1 when detonation was successful and consistent. An explanation for the consistently low impulse is the mixing and over-expansion of the main tube charge during the filling process in multi-cycle operation. Although a predetonator is effective, an oxygen-rich predetonator may not be practical outside of the laboratory because of the difficulty and bulk of storing or generating oxygen.

This sensitivity to initiation strategy also limits the methods of detonation initiation acceptable for an engine. The effect of the length and volume of DDT mechanism was shown through the performance as well as by the reduced head pressure (likely caused by the retonation wave passing through the DDT mechanism.) In general, the initiation volume for DDT should be less than 10% of the total tube volume. The implication is that detonation initiation, for all practical fuels and devices, must be accomplished somewhere other than the main detonation tube where effects of confinement can be maximized and obstacle drag can be minimized.

Detonation initiation for hydrocarbon or insensitive fuel continues to remain an area requiring innovations. Research is needed to develop low drag DDT mechanisms and air-fuel predetonators.

Acknowledgments

This work would not have been possible without the technicians who worked on this project; our thanks to Curtis Rice, Dave Baker, and Dwight Fox (ISSI). Dr. Tim Edwards (AFRL/PRTG) was extremely helpful in developing the fuel systems for this work. The authors would also like to thank Jeff Stutrud (AFRL/PRTC) for his controls and data acquisition expertise and Jacquelyn Kimmel for her help. The technical leadership of Dr. Mel Roquemore and Dr. Robert Hancock (AFRL/PRTC) was invaluable. Funding was provided by the Air Force Research Laboratory, Propulsion Directorate and AFOSR.

References

1. S. Jackson and J. Shepherd, "Initiation Systems for Pulse Detonation Engines," AIAA-2002-3627 38th AIAA/ASME/SAE/ASEE Joint Propulsion Conference and Exhibit, Indianapolis, IN, July 7-10, (2002).
2. J. Sinibaldi, J. Rodriguez, B. Channel, C. Brophy, F. Wang, C. Cathey, and M. Gundersen, **"**Investigation of Transient Plasma Ignition For Pulse Detonation Engines," Los Angeles, CA AIAA-2005-3774, 41st AIAA/ASME/SAE/ASEE Joint Propulsion Conference and Exhibit, Tucson, AZ, July 10-13, (2005).
3. C. M. Brophy, J. O. Sinibaldi, and P. Damphousse, "Initiator performance for liquid-fueled pulse detonation engines," AIAA-2002-472 AIAA Aerospace Sciences Meeting and Exhibit, 40th, Reno, NV, Jan. 14-17, (2002).
4. S. Jackson and J. Shepherd, "Detonation Initiation via Imploding Shock Waves," AIAA-2004-3919 40th AIAA/ASME/SAE/ASEE Joint Propulsion Conference and Exhibit, Fort Lauderdale, FL, July 11-14, (2004).
5. F. Schauer, C. Miser, C. Tucker, R. Bradley, and J. Hoke, "Detonation Initiation of Hydrocarbon-Air Mixtures in a Pulsed Detonation Engine," AIAA-2005-1343 43rd AIAA Aerospace Sciences Meeting and Exhibit, Reno, NV (2005).
6. J.L. Hoke, R.P. Bradley, F.R. Schauer, "Impact of DDT Mechanism, Combustion Wave Speed, Temperature and Charge Quality on Pulsed Detonation Engine Performance," AIAA 2005-1342, 43rd AIAA Aerospace Sciences Meeting, Reno, NV (2005).
7. K. Kailasanath, "On the Performance of Pulse Detonation Engines," presented at *The International Colloquium on Advances in Confined Detonations*, Moscow (2002).
8. Cooper, M., Jackson, S., Austin, J., Wintenberger, E., and Shepherd, J. E., "Direct Experimental Impulse Measurements for Detonations and Deflagrations," Journal of Propulsion and Power, Vol. 18, No. 5, pp. 1033–1041 (2002).
9. F. R. Schauer, J.S. Stutrud, and R.P. Bradley, "Detonation Initiation Studies and Performance Results for Pulsed Detonation Engine Applications, "AIAA 2001-1129, 39th AIAA Aerospace Sciences Meeting, Reno, NV (2001).
10. E. Schultz, E. Wintenberger, and J. Shepherd, "Investigation of Deflagration to Detonation Transition for Application to Pulse Detonation Engine Ignition Systems," 16th JANNAF Propulsion Meeting (1999).
11. Soloukhin, R. I., Shock Waves and Detonations in Gases, Mono Book Corp, Baltimore (1963).
12. Kristin L. Panzenhagen, Paul I. King, Colin K. Tucker, and Fred R. Schauer, "Liquid Hydrocarbon Detonation Branching in a Pulse Detonation Engine," AIAA-2004-3401, Ft Lauderdale, FL (2004).
13. E. Wintenberger, J. M. Austin, M. Cooper, S. Jackson, and J. E. Shepherd, "An analytical model for the impulse of a single-cycle pulse detonation engine," AIAA-2001-3811 AIAA/ASME/SAE/ASEE Joint Propulsion Conference and Exhibit, 37th, Salt Lake City, UT, July 8-11, (2001)
14. Cooper, M., Shepherd, J., and Schauer, F., "Impulse correlation of partially filled detonation tubes," Journal of Propulsion and Power 0748-4658 vol.20 no.5, pp 947-950 (2004).
15. T. R. Meyer, M. S. Brown, J. L. Hoke, J. T. Parker, J. R. Gord and F. R. Schauer, "Fiber-Coupled Laser Sensor for In-Situ Measurement of Hydrocarbon Fuels in Pulsed-Detonation Engines," 28th Annual Dayton-Cincinnati Aerospace Sciences Symposium, Dayton, OH, 4 March (2003).
16. J. E. Shepherd, E. Schultz and R. Akbar, ``Detonation Diffraction," *the 22nd International Symposium on Shock Waves*, Imperial College, London, UK, pp. 41-48, (2000).
17. Katta, V.R., Chin, L.P., and Schauer, F. "Numerical studies on cellular detonation wave subjected to sudden expansion," 17th International Colloquium on the Dynamics of Explosions and Reactive Systems, July 25-30, Heidelberg, Germany (1999).

Cycle Performance of a Pulse Detonation Engine with Supercritical Fuel Injection

Pulse detonation engines (PDEs) rely on rapid ignition and formation of detonation waves. Because hydrocarbon fuels are composed typically of long carbon chains that must be reduced in the combustion process, it would be beneficial to create such reduction prior to injection of fuel into the engine. This study focused on PDE operation enhancements using dual detonation tube, concentric-counter-flow heat exchangers to elevate the fuel temperature up to supercritical temperatures. Variation of several operating parameters included fuel type (JP-8, JP-7, JP-10, RP-1, JP-900, and S-8), spark delay, and firing frequency. To quantify the performance, four key parameters examined were ignition time, deflagration to detonation transition (DDT) time, detonation distance, and the percent of ignitions resulting in a detonation. In general, for all fuels except JP-10, increasing the fuel injection temperature decreased DDT time and detonation distance, increased the percent of ignitions resulting in detonations (detonation percentage), and had no impact on ignition time. JP-10 was difficult to detonate, resulting in extremely poor performance. An increase in cycle frequency resulted in a decrease in DDT time, but had little effect on ignition time and detonation distance. Analysis of spark delay showed that 4 msec is the best spark delay at high fuel injection temperatures, based on total time to detonation and detonation percentage.

Nomenclature

A	=	Arrehenius Constant
E_a	=	Activation Energy
E_{crit}	=	Critical Initiation Energy
[fuel]	=	Concentration of Fuel
[oxidizer]	=	Concentration of Oxidizer
P	=	Head Pressure
RR	=	Reaction Rate
R_u	=	Universal Gas Constant
T_{mix}	=	Fuel/Air Mixture Temperature
λ	=	Cell Size

VI. Introduction

WHILE the pulse detonation engine has the potential to provide significant advantages over current aircraft propulsion systems, it is still in the early stages of development. Several technological barriers need to be overcome before the PDE can be considered a practical means of providing propulsion to operational aircraft[1,2]. A large hurdle is the efficient use of low vapor pressure hydrocarbon fuels, such as JP-8, JP-7, JP-10, JP-900[*], RP-1, and S-8[†]. The vast majority of research into pulse detonation engines has been performed with gaseous fuels, such as hydrogen and simple hydrocarbons[3]. The lack of liquid hydrocarbon fuel research has left a large gap between research and the operational use of pulses detonation engines. While gaseous fuels are readily available for research, nearly all United States Air Force (USAF) aircraft and air-breathing missiles utilize liquid fuels, primarily JP-8 and JP-10. Therefore, the ability to utilize liquid

[*] The fuel referred to as JP-900 in this paper is a coal-derived liquid hydrocarbon fuel developed at The Penn State University. It is denoted as JP-900 due to its thermal stability to 900 ºF.

[†] S-8 is a synthetic fuel derived from natural gas via the Fischer-Tropsch process. S-8 is also referred to as Fischer-Tropsch JP-8 or just Fischer-Tropsch.

hydrocarbon fuels efficiently in the PDE is necessary to bring pulse detonation engine technology out of the research phase and into operation.

Four key cycle parameters are adversely affected by using liquid hydrocarbon fuels in lieu of gaseous fuels. The parameters are the time it takes to create a deflagration wave within the fuel/air mixture (ignition time), the time it takes to transition the deflagration wave into a detonation wave (DDT time), the length of detonation tube required for the mixture to transition to a detonation (detonation distance), and the consistency of the detonations (detonation percentage). Both the ignition time and the DDT time are nearly an order of magnitude larger for complex liquid hydrocarbon fuels than simpler gaseous fuels. For example, ignition time for a hydrogen/air mixture is on the order of one millisecond, where as the ignition time of a JP-8/air mixture is near seven milliseconds.

The cycle performance of a liquid hydrocarbon fueled PDE with fuel injection temperatures above the flash vaporization point is unknown. Previous research has demonstrated that flash vaporization of liquid hydrocarbon fuels significantly improved the PDE performance, but no research has been conducted to determine the effect of operating with fuel injection temperatures beyond the point of flash vaporization[4]. The focus of this research is to use a dual concentric counter-flow heat exchanger system to determine the effect of fuel injection temperature on the ignition time, DDT time, detonation distance, and detonation percentage with varying operating parameters. The operating parameters examined include; fuel type (JP-8, JP-7, JP-10, JP-900, RP-1, and S-8), spark delay and frequency[5].

VII. Background and Theory

A. Global Reaction Theory

Global reaction theory assumes that the reaction of a fuel/air mixture can be modeled as a single global reaction. Low vapor pressure fuel/air mixture combustion is not governed by a single global reaction; however, global reaction theory can be used to predict ignition trends. The ignition time is inversely related to the reaction rate, where the reaction rate is determined by the Arrehenius expression (Eq. 1)

$$IgnitionTime \propto \frac{1}{RR} = \frac{1}{A} P^{-n} [fuel]^{-m} [oxydizer]^{-j} e^{\left(\frac{E_a}{R_u T_{mix}}\right)} \tag{1}$$

where n, m, and j are experimentally determined constants[6]. Based on Eq. 1, the reaction rate of a fuel-air mixture will increase with increasing mixture temperature and head pressure. The ignition time is inversely related to the reaction rate; hence, as the mixture temperature or head pressure increases the ignition time will decrease. However, for the small percentage that the fuel/air mixture temperature is increased, there is no noticeable ignition time decrease expected.

B. Cell Size and Critical Initiation Energy

Previous experimental research has shown that a typical stoichiometric low vapor pressure liquid hydrocarbon/air mixture requires on the order of 10^5 J of energy to directly initiate detonation, six orders of magnitude greater than the energy available form a typical spark plug (~100 mJ). Figure 1 is a plot of cell size versus direct initiation detonation energy for several stoichiometric fuel/oxydizer mixtures[7]. From a best-fit curve through the data, a simple relationship between the cell size and critical initiation detonation energy is shown on Figure 1. The important item to notice is the critical initiation energy varies with the cube of the cell size.

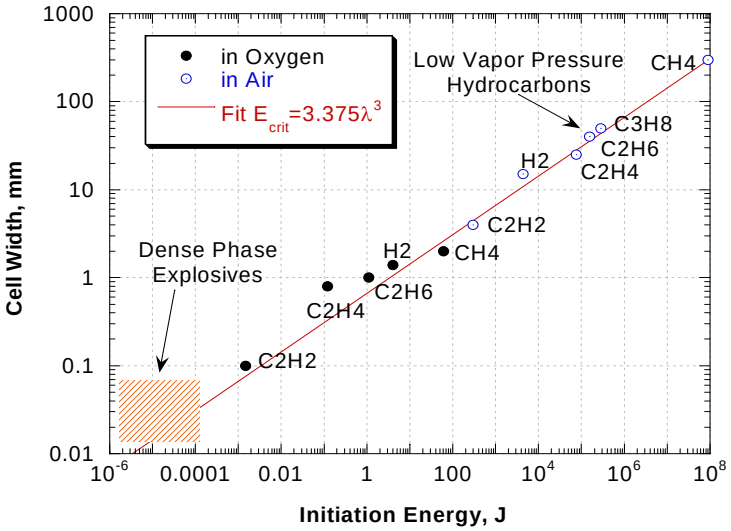

Figure 1. Experimentally determined relationships between cell size and critical initiation energy for various stoichiometric fuel/oxidizer mixtures[7]

C. Spark Delay and Initial Pressure

The PDE head pressure fluctuates due to the presence of compression and expansion waves in the detonation tube. These waves are created as the fill and purge air is forced into the detonation tubes. By selection of a spark delay, it is possible to deposit the spark during a compression wave, when the head pressure is above ambient. Figure 2 is the pressure time history during the PDE fire phase without combustion at 15 Hz with a mixture temperature of 394 K (250 ˚F). Spark delays of 2, 4, 6, 8, and 10 msec are denoted as vertical lines in Figure 2.

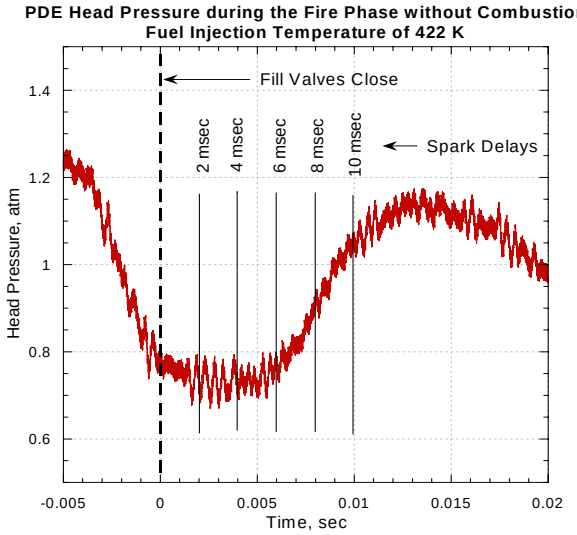

Figure 2. PDE head pressure during fire phase without combustion (vertical lines denote various spark delays)

Figure 2 demonstrates the benefit of selecting a high spark delay. Selection of a 6, 8, or 10 msec spark delay allows combustion to occur during a compression wave, while a 0 msec spark delay forces combustion to occur during an expansion wave. The ignition time is not only affected by the pressure when the spark is deposit. The entire pressure history during the formation of a deflagration wave directly affects the ignition time. The time it takes for a deflagration wave to form following the spark (ignition time) is approximately 7

msec for JP-8. Therefore, the average pressure over the 7 msec following the deposit of the spark was determined for all spark delays from Figure 2, and is shown in Table 1.

Table 1. Initial head pressure and average head pressure occurring over the 7 msec following the spark deposit

Ignition Delay [msec]	Initial Pressure [atm]	Average Pressure [atm]
2	0.712	0.819
4	0.728	0.907
6	0.765	1.005
8	0.932	1.079
10	1.042	1.105

Table 1 can be used to determine the potential effect of spark delay for a fuel injection temperature of 394 K. The difference between the average pressure of the 2 msec and 10 msec spark delay cases is 0.286 atm, or 25.9%. This difference is substantial, meaning that a large difference in ignition time is expected between the 2 msec and the 10 msec cases. A difference in ignition time is also expected between the 4 msec and the 10 msec cases, but it will be less than the difference between the 2 msec and the 10 msec cases. The 6, 8, and 10 msec spark delays should produce similar ignition times, because the maximum difference between their average head pressures is 0.100 atm or 9%.

D. Effect of Initial Pressure and Temperature on Detonability

Little research has been performed to determine the relationship between initial mixture properties (temperature and pressure) and the detonability of a low vapor pressure fuel/air mixture. Literature is available for lighter hydrocarbon/oxidizer mixtures[7]. The cell size of three different light hydrocarbons as a function of initial mixture temperature is shown in Figure 3(a). Figure 3(b) is a plot of initial pressure versus cell size for three light hydrocarbon/oxydizer mixtures and one H_2/O_2 mixture.

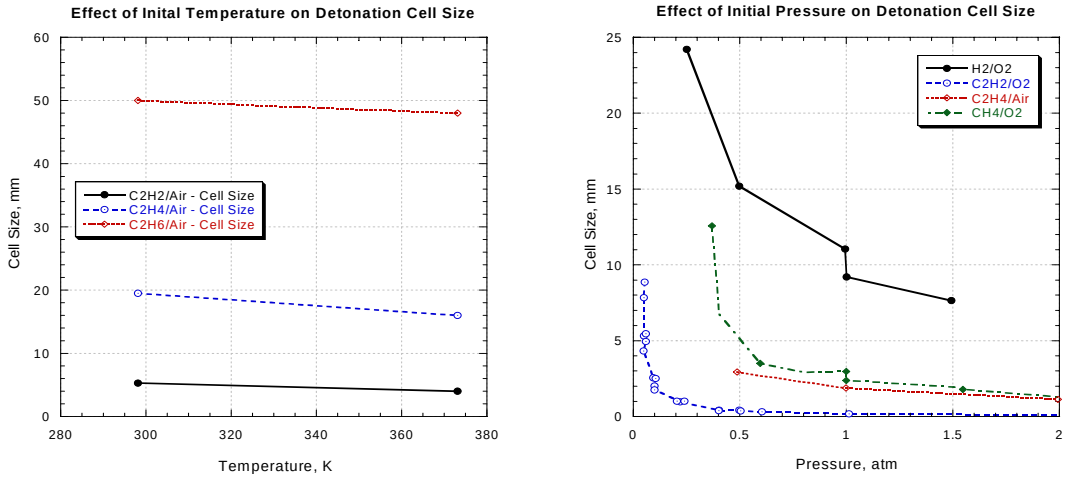

(a) (b)

Figure 3. Effect of initial temperature (a) and initial pressure (b) on detonation cell[7]

The trend of these hydrocarbons is for the cell size to decrease with increased mixture temperature and head pressure. The three hydrocarbons examined in Figure 3(a) are all very light compared to low vapor pressure liquid hydrocarbons, with only two carbon atoms apiece. While the trends of smaller hydrocarbons do not dictate the trends of much heavier hydrocarbon, they do suggest that increasing initial mixture temperature and/or head pressure will decrease the cell size. The decrease in cell size is an indication of an increase in performance. According to the curve fit equation inset in Figure 1, the critical initiation energy

decreases by the cube of the cell size. As the critical initiation energy decreases, the detonability of the mixture will increase. It is expected that increases in both initial head pressure and initial mixture temperature will result in decreased DDT time and detonation distance, as well as increased percentage of ignitions resulting in detonations.

VIII. Experimental Setup and Instrumentation

A. Facilities and PDE Specifics

This research was conducted at the Pulse Detonation Research Facility located in Building 71A, D Bay, Wright Patterson AFB, Ohio (D-Bay). This facility is described in detail in other literature, and only the details relevant to this effort have been provided[3]. The PDE for this research consisted of a GM quad four head with two 1.83 meter long schedule 40 stainless steel detonation tubes (5.08 cm radius); each with a 0.91 meter structurally modified Schelkin spiral to promote DDT[8]. The PDE was setup with two detonation tubes, each with a stainless steel heat exchanger. Detonation tubes one and four were used for all tests.

The PDE cycle consisted of three equally timed phases. The three phases, in order, are the fill, fire, and purge phases. During the fill phase the intake valves were opened filling the PDE thrust tube with a volume of premixed fuel/air mixture equal to the volume of the thrust tube (fill fraction of one). For all tests the fill air was initially heated to 394 K prior to mixing with the fuel. For the fire phase an automotive ignition system provided four spark pulses through modified NGK spark plugs providing ignition energies of 420-460 mJ. The spark delay after the intake valves closed was 4 msec, unless otherwise noted. The fire provided sufficient time for the spark delay, ignition, DDT, and blowdown. During the purge phase the exhaust valves were opened filling the thrust tube with a volume of air equal to half the volume of the detonation tube (purge fraction of 0.5). The purge air cooled the thrust tube and removed a portion of the exhaust gases from the thrust tube preventing backfiring. The PDE firing frequency was varied throughout test, but remained between 10 and 20 Hz.

B. Supercritical Fuel Heating System

The liquid fuel required for this testing was supplied by two hydraulic bladder accumulators, pressurized by high-pressure nitrogen bottles. The nitrogen bottles pressurized the fuel above the critical pressure for the entire duration of the test to prevent boiling. The fuel was pressure fed to the inlet of the supercritical fuel heating system (SFHS). The SFHS consisted of a nitrogen purge system, two stainless steel heat exchangers, fuel filter assembly, Delavan aerospace nozzles, instrumentation, and associated tubing and fittings necessary to connect the critical components. The fuel filter was necessary to remove the small amounts of coking that is formed due to endothermic cracking of the fuel[9]. The fuel enters the test stand through a ball valve where the flow is split into two fuel lines. One fuel line leads to the inlet of the heat exchanger on tube four, while the other fuel line leads to the inlet of the heat exchanger on tube one. After the two fuel paths have exited their respective heat exchanger, they are teed back together. The fuel is then led through the filter to the fill air manifold, where it is injected into the air stream via the Delevan aerospace nozzles. The fuel lines that carry heated fuel (fuel that has traversed through a heat exchanger) are insulated with fiberglass insulation. The flow path and instrumentation are shown in schematic and photograph form in Figure 4(a) and Figure 4(b), respectively.

Fuel mass flow rate of the nozzles was proportional to the square root of the pressure drop across the fuel nozzles and fuel density[10,11]. To compensate for the decrease in fuel density during heating of the fuel in the supercritical regime, the charge pressure of the accumulators was increased to maintain a constant fuel mass flow rate. To allow for variations in accumulator charge pressure during testing, a pneumatic dome loader was installed for nitrogen pressure regulation.

To minimize carbon deposition in the SFHS, the JP-8 was de-oxygenated through a nitrogen sparging process. The sparging process involved bubbling a volume of nitrogen through the JP-8 which displaced the oxygen from the fuel. The volume of nitrogen necessary to reduce the oxygen concentration to acceptable levels was determined experimentally in previous work, and to ensure acceptable levels a factor of safety of two was applied to all nitrogen volume calculations[2,12].

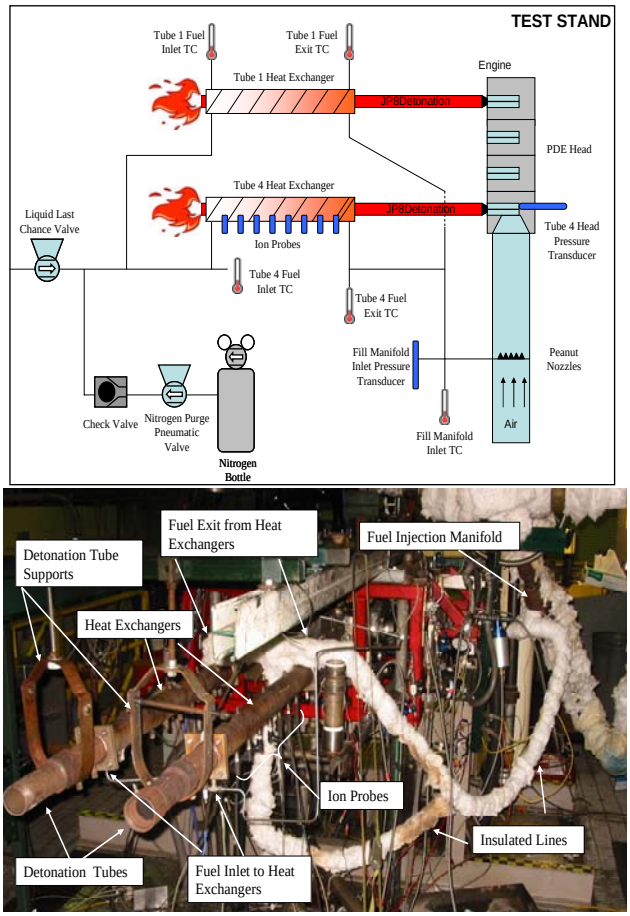

(a) (b)

Figure 4. (a) Diagram and (b) photograph of the PDE with the supercritical fuel heating system and instrumentation

C. Heat Exchangers

Two identical concentric tube heat exchangers were fabricated for this work. A 0.91 meter heat exchanger was fabricated with 5.08 cm dia, type 316 stainless steel, schedule 40 inner tube and 6.35 cm dia, type 316 stainless steel, schedule 40 outer tube allowing for a 1.22 mm annular thickness. A photograph of one heat exchanger and the associated instrumentation ports are shown in Figure 5.

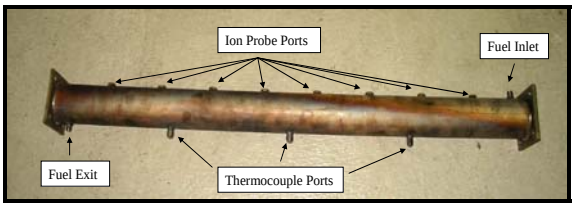

Figure 5. Photograph of one heat exchanger

D. Nitrogen Purge System

A nitrogen purge system was designed to prevent supercritical fuel from remaining in the heat exchangers at the end of a test[13]. The nitrogen purge system consists of a high-pressure nitrogen bottle, manual pressure regulator, pneumatic valve, check valve, and ball valve. Before testing began, the ball valve was opened to allow for operation of the nitrogen purge system. The manual pressure regulator was set above the critical pressure of the fuel. The pneumatic valve is placed in the nitrogen purge line to commence and terminate the nitrogen flow. The pneumatic valve can be activated remotely during testing. Once a test has ended, the pneumatic valve is opened allowing the nitrogen to purge the heat exchangers of supercritical fuel. A check valve is located directly after the pneumatic valve to prevent fuel from entering the nitrogen line.

E. Instrumentation

Temperature was measured at the inlet and outlet of each heat exchanger, inlet to the fill air manifold, and inlet to the head using thermocouples placed in the center of the flow path. External heat exchanger wall temperatures were measured with J-type thermocouples mounted externally by compression clamps to the PDE detonation tube. A pressure transducer was situated in the head cavity of tubes one and four to gather the head pressure data used to determine the ignition time. Ion probes were placed in the ion probe ports in both the tube one and four heat exchangers[14].

F. Uncertainty Analysis

The total experimental uncertainty is determined by combining the bias and precision uncertainties using the root sum square[15]. The bias uncertainties are constant for all data points of the same variable, while the precision uncertainties vary for each data point. Therefore, the total experimental uncertainty will vary by data point. A comprehensive bias uncertainty analysis was performed, and the results are displayed in Table 2.

Table 2. Summary of bias uncertainties for experimental results

Experimental Result	Bias Uncertainty
Wavespeed	± 55.12 m/s
Ignition Time	± 0.292 msec
DDT Time	± 0.0568 msec
Detonation Distance	± 0.0568 m
Fuel Injection Temperature	± 3.6 K
Fuel/Air Mixture Temperature	± 2.5 K
Equivalence Ratio	± 0.0147

IX. Results and Discussion

The analysis of various operating parameters for increasing fuel injection temperature is presented. The results include ignition time, deflagration to detonation time, detonation distance, and detonation percentage, with all parameters plotted versus fuel injection temperature. Each data point represents the mean value of 40 to 60 ignitions, using data from two tubes. The standard deviation is presented whenever possible. . The effect of fuel injection temperature on the performance of the PDE with variation of the following operating parameters is shown: Fuel selection, spark delay, and firing frequency.

A. Fuel Study

Figure 6 is a plot of (a) ignition time and (b) DDT time as a function fuel injection temperature for all six fuels. No differentiation amongst the fuels can be made. JP-8 has a noticeably higher ignition time in the range of 586 to 755 K. The probable cause of this trend is adverse effects of thermal degradation of the JP-8. In addition, S-8 produced the lowest ignitions for almost the entire temperature range. JP-7, JP-900, and RP-1 demonstrate almost no difference in trend or magnitude, which was expected due the similarity of the fuels. With the exception of JP-8, ignition times for all fuels are independent of fuel injection temperature in the temperature range examined, as expected based on global reaction theory.

It was found that detonation of a JP-10/air mixture was very difficult with the current setup. Do to the lack of detonations, the DDT time and detonation distance data for JP-10 was heavily scattered. The atrocious precision of the JP-10 detonation data renders the DDT time and detonation location results for JP-10 unusable. Therefore, the DDT time and detonation distance results for JP-10 have been omitted. The DDT time for the other five fuels is displayed in Figure 6(b) as a function of fuel injection temperature.

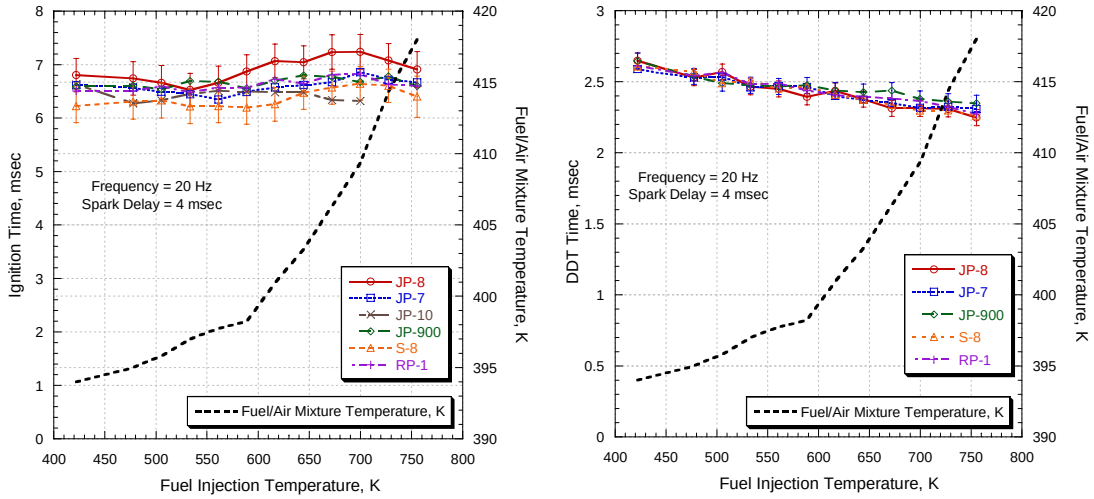

(a) (b)

Figure 6. (a) Comparison of the ignition time for six fuels as a function of fuel injection and (b) comparison of the DDT time for six fuels as a function of fuel injection temperature

No stratification is seen between the fuels with regards to the DDT time. The difference between any two fuels is within the experimental error for the entire temperature range. All five fuels are inversely related to fuel injection temperature, as expected. A nearly linear trend is shown for each fuel with approximately a 15% decrease in DDT time over the temperature range.

The next parameter analyzed was the detonation distance. The detonation distance as a function of fuel injection temperature for all fuels other than JP-10 is shown in Figure 7(a). As expected, the detonation distance of all five fuels demonstrates an inverse relationship with fuel injection temperature. Below 644 K the detonation distance of the five fuels differs in both magnitude and slope, but above 644 K the fuels produce identical detonation distances. The fuels show significant stratification below 644 K. JP-8 has the lowest detonation distances, followed closely by JP-900. JP-7 performs the poorest above 644 K, with a maximum value of 1.14 m. RP-1 and S-8 perform very similarly, both with detonation distance between JP-7 and JP-900. Once the individual fuels reach flash vaporization temperatures, detonations occur very close to the end of the spiral.

The detonation percentage is shown in Figure 7(b) as a function of fuel injection temperature. Again, the detonation percentage is the percentage of ignitions that result in a combustion wavespeed of 1800 m/s or greater. All fuels demonstrate a strong trend of increasing detonation percentage for an increase in fuel injection temperature. JP-7 and S-8 stand out as the fuels that produce the largest percentage of detonations. The fuels can be lumped into three categories, based on Figure 7(b). The first group, JP-7 and S-8, demonstrate remarkable increases in detonations as fuel injection temperature increases. Both JP-7 and S-8 provide nearly 100% detonations at 755 K. JP-8, JP-900, and RP-1 make up the second category; they all demonstrate very similar trends for the percentages. JP-8, JP-900, and RP-1 produce detonation percentages between 65 and 75% at a fuel injection temperature of 755 K. The final category includes only JP-10. While JP-10 demonstrates an increase in detonation as fuel injection temperature is increased, the magnitude of the detonation percentage remains undesirable. The detonation percentage of JP-10 increases from 14 to only 38%. These meager detonation percentages led to the large uncertainty in DDT time and detonation distance data for JP-10/air mixtures.

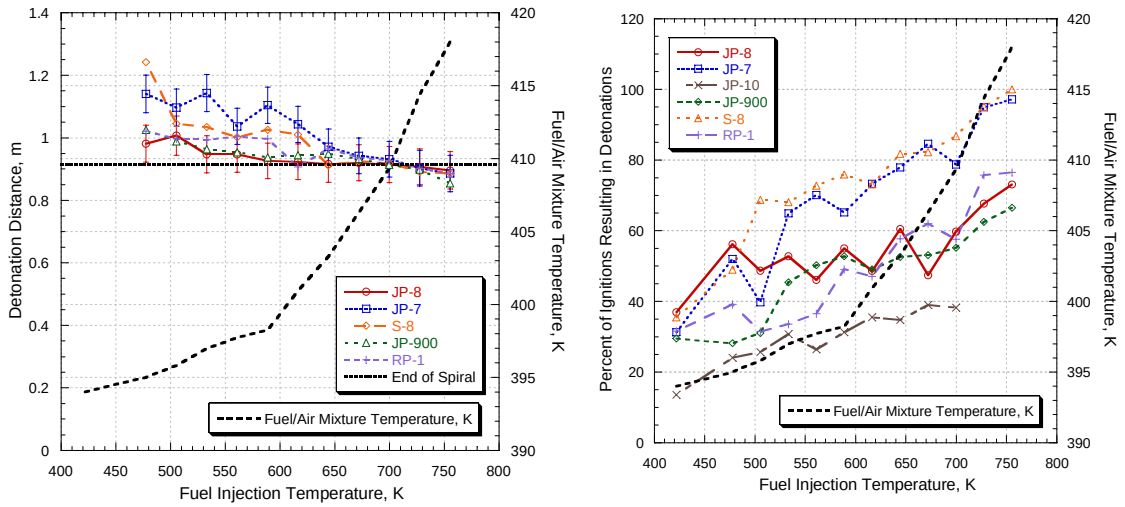

Figure 7. (a) Comparison of the detonation distance for five fuels as a function of fuel injection and (b) comparison of the detonation percentage for six fuels as a function of fuel injection

Table 3 is a summary of the important values determined during the fuels study. While these values are taken directly from Figure 6 and Figure 7, the table was added for quick reference. Since the ignition time was shown to be constant for all fuel other than JP-8, an average value is presented in Table 3. DDT time, detonation distance, and detonation percentage all demonstrated nearly linear relationships with fuel injection temperature; therefore, the maximum and minimum values are presented in Table 3.

Table 3. Summary of important performance parameter values determined during fuels study

Fuel	Average Ignition Time [msec]	Maximum DDT Time [msec]	Minimum DDT Time [msec]	Maximum Detonation Distance [m]	Minimum Detonation Distance [m]	Maximum Detonation Percentage	Minimum Detonation Percentage
JP-8	6.90	2.65	2.25	1.00	0.90	36.9	73.1
JP-7	6.59	2.59	2.31	1.14	0.89	31.3	97.2
JP-10	6.43	N/A	N/A	N/A	N/A	13.6	38.3
JP-900	6.63	2.65	2.35	1.03	0.85	29.5	66.5
RP-1	6.62	2.61	2.27	1.02	0.89	31.6	76.5
S-8	6.37	2.61	2.26	1.02	0.89	35.5	100.0

B. Spark Delay

To determine the effect of varying spark delay, a series of tests were performed for varying spark delays. All spark delay testing was performed with JP-8 as the fuel. Do to the time constraints of the fire phase, a frequency of 15 Hz was used for all spark delay testing. By selecting a frequency of 15 Hz, spark delays of up to 10 msec could be tested safely. Spark delays of 0, 2, 4, 6, 8 and 10 msec were examined. The 0 msec spark delay case resulted in constant backfiring of the PDE, therefore no data was taken.

Figure 8(a) is a plot of the ignition time as a function of fuel injection temperature for a JP-8/air mixture with spark delays ranging from 2 to 10 msec. With the exception of the 2 msec spark delay case, there is no significant stratification, especially at low temperatures. The 2 msec spark delay results demonstrate significantly higher ignition times for all temperatures as compared to the other spark delays, as expected based on global reaction theory. The 4 msec case produces slightly higher ignition times at low temperatures, but lower spark delays at higher temperature. The spark delays between 6 and 10 msec do not show significant

stratification amongst each other. It should be noted that the difference between the 4 msec case and the higher spark delay cases is within the experimental error at temperatures below 589 K.

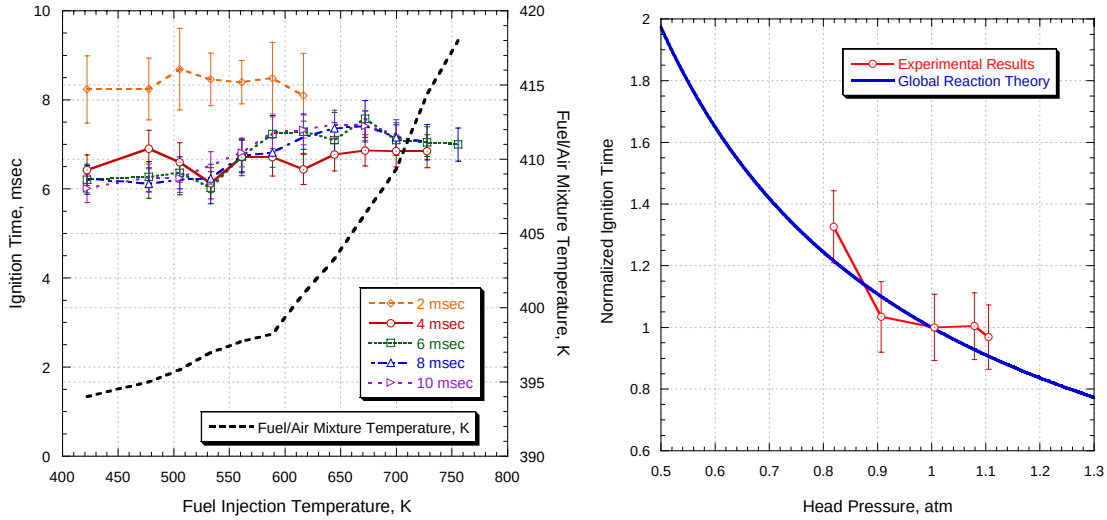

(a) (b)

Figure 8. (a) Ignition for varying spark delays as a function of fuel injection temperature for a JP-8/air mixture and (b) comparison of experimental and theoretical ignition time as a function of head pressure for a JP-8/air mixture – frequency = 15 Hz

The ignition time for each spark delay at 422 K can be used to determine the accuracy of the global reaction theory at low fuel injection temperatures. The global reaction theory approximation (discussed in Section II-A) for normalized ignition time as a function of average head pressure is shown in Figure 8(b). Along with the global reaction theory approximation, the experimentally determined normalized ignition time as a function head pressure is displayed in Figure 8(b). The experimentally determined ignition times at 422 K are taken from Figure 8(a) as a function of spark delay. The spark delay corresponds to an average head pressure, from Table 1. The ignition times were normalized by the ignition time corresponding to a spark delay of 6 msec, because the average head pressure of the 6 msec case is within 1% of ambient pressure.

Figure 8(b) shows that the experimental results compare well with global reaction theory. The global reaction theory approximation is within the experimental uncertainty of the experimental mean. This is an analysis of global reaction theory only at a fuel injection temperature of 422 K. No conclusion is made about the validity of global reaction theory at very high fuel injection temperatures.

Figure 9(a) is a plot of the DDT time for a JP-8/air mixture as a function of fuel injection temperature for various spark delays. The 2 msec spark delay trials resulted in sporadic and meager detonations, leading to extremely poor confidence in results. Therefore, the DDT time and detonation distance data is not presented. All other spark delays demonstrate the same trend, where increasing fuel injection temperature leads to decreasing DDT time. It is also apparent that increasing the spark delay will reduce the DDT time. The DDT time was expected to decrease with increasing head pressure, based on the light hydrocarbon/air detonation data (shown in Section II-D).

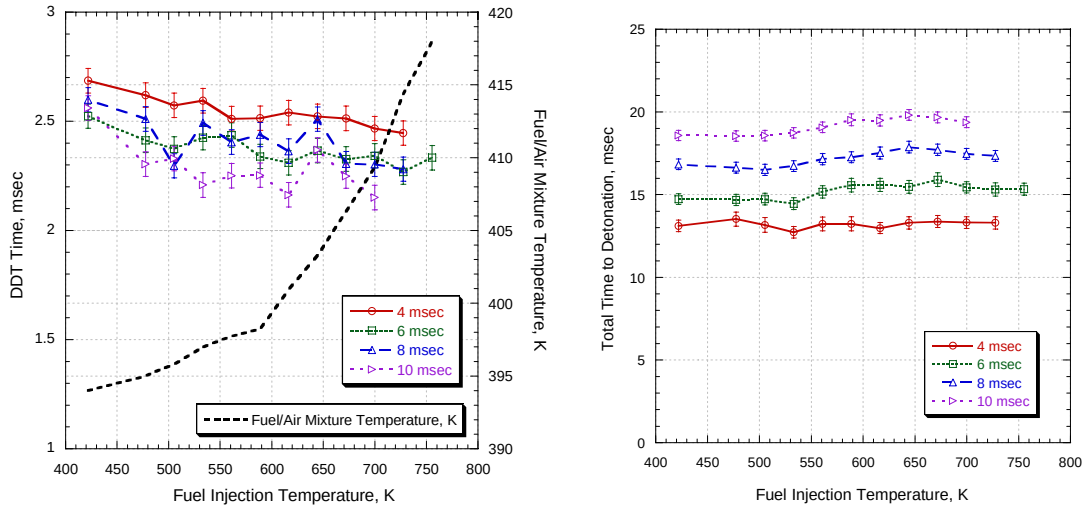

(a) (b)

Figure 9. (a) DDT time for a JP-8/air mixture as a function of fuel injection temperature for varying spark delays and (b) Total time to detonation for a JP-8/air mixture as a function of fuel injection temperature for various spark delays – frequency = 15 Hz

To compare the overall effect of varying spark delays in a PDE, the total time to detonation is plotted as a function of fuel injection temperature for various spark delays in Figure 9(b). The total time to detonation is the sum of the spark delay, ignition time, and DDT time. The reduction in ignition time and DDT time as spark delay is increased is overshadowed by the increase in spark delay. Therefore, a spark delay of 4 msec produces the lowest total time to detonation, and a spark delay of 10 msec produces the highest total time to detonation.

Figure 10(a) is a plot of the detonation distance of a JP-8/air mixture as a function of fuel injection temperature for various spark delays. The four spark delays all show an inverse relationship with fuel injection temperature. The 4 msec spark delay case stands out with the lowest detonation distance for all fuel injection temperatures; although, the difference between the 4 msec spark delay and the higher spark delays is within the experimental error. The other three spark delays are nearly identical, especially at the lower temperatures.

Figure 10(b) is a plot of the detonation percentage of a JP-8/air mixture as a function of fuel injection temperature for various spark delays. The detonation percentage is significantly impacted by the spark delay. The detonation percentage increases steadily as the spark delay decreases. The 10 msec spark delay results in detonation percentages ranging from 13.3 to 37.7%, while the spark delay for the 4 msec case increases from 33.3 to 95.0%. In fact, the detonation percentage for the 4 msec spark delay is near 90% for all fuel injection temperatures above 505 K.

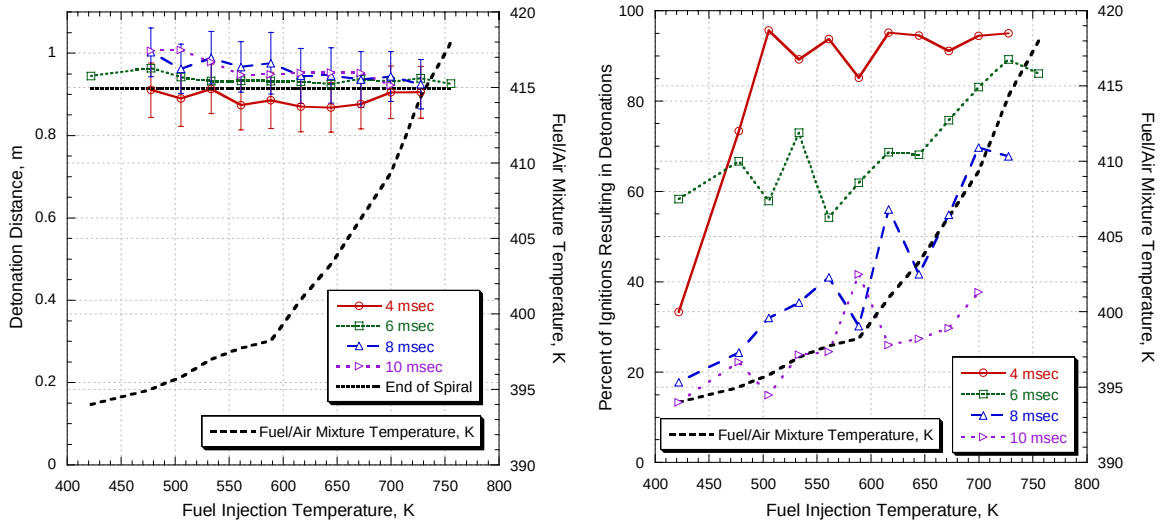

(a) (b)

Figure 10. (a) Detonation distance for a JP-8/air mixture as a function of fuel injection temperature for varying spark delays and (b) detonation percentage as a function of fuel injection temperature for various spark delays using a JP-8/air mixture – frequency = 15 Hz

C. Frequency

The motivation to decrease ignition time and DDT time is to decrease the fire phase time, thus decreasing the PDE cycle time. If the cycle time is decreased then the PDE firing frequency can be increased, thereby increasing thrust. This rationale hinges on the assumption that increasing the frequency will not produce any adverse effects on PDE cycle performance. To demonstrate that increasing the frequency will not hinder PDE performance, a study was conducted with three frequencies. Frequencies of 10 Hz, 15 Hz, and 20 Hz were tested to determine the ignition time, DDT time, detonation distance. Frequencies above 20 Hz are not possible at this time due to limitations of the length of the fire cycle. A system operating at 25 Hz allows only 13.3 msec to be spent on the fire cycle; this time limit is too short for the detonation of a JP-8/air mixture. The 10 Hz frequency did not provide enough energy to the system to afford fuel injections temperatures above 644 K. The inability to heat the fuel to adequate temperatures using a frequency of 10 Hz prohibited proper comparison with other frequencies, therefore the 10 Hz results have been omitted.

Figure 11(a) is a plot of ignition time and DDT time as a function of fuel injection temperature for a PDE operating at 15 Hz and 20 Hz. The frequencies show nearly identical ignition times for the entire temperature range. The difference between the results using the two frequencies is within the experimental error. The DDT time for the 20 Hz case is less than the DDT time for the 15 Hz case for the entire temperature range, especially at higher temperatures. The total time to detonation (sum of ignition time and DDT time) for the 20 Hz case is less than for the 15 Hz case. This demonstrates an improvement in performance with increasing frequency.

Figure 11(b) is a plot of the detonation distance as a function of fuel injection temperature with varying frequency. The difference between the detonation distance results of the 15 and 20 Hz tests are within the error for the entire temperature range. In addition, both frequencies result in detonations at the end of the internal spiral. Again, no degradation in performance is noticed when operating at 20 Hz as compared to at 15 Hz. Therefore, increasing the frequency was found to induce an increase in cycle performance.

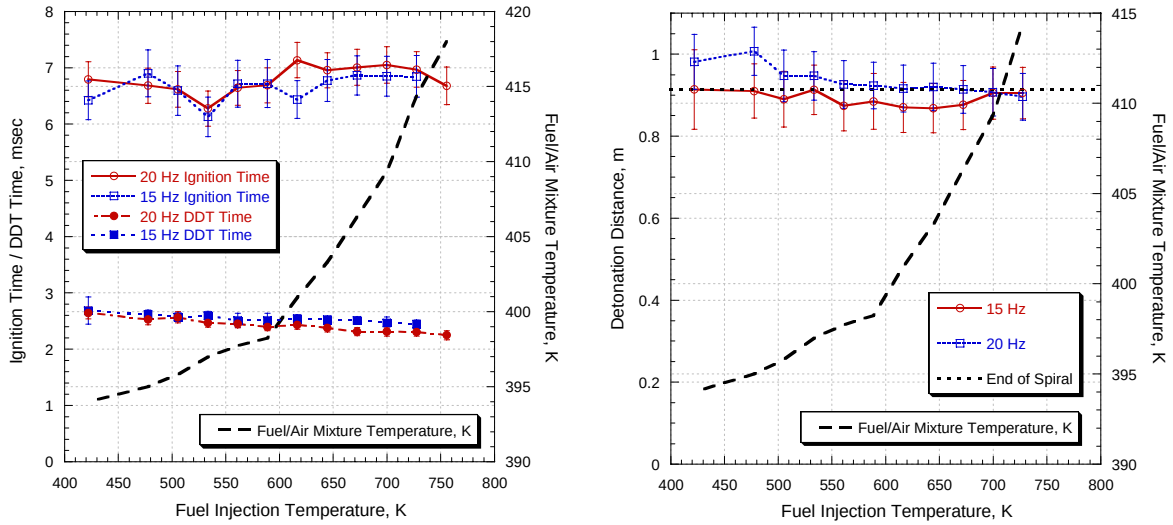

(a) (b)

Figure 11. (a) Comparison of ignition time and DDT time for two frequencies as a function of fuel injection temperature for a JP-8/air mixture and (b) Comparison of detonation distance for two frequencies as a function of fuel injection temperature for a JP-8/air mixture – spark delay = 4 msec

X. Conclusions

This research marked the first analysis of the effect of increasing fuel injection temperature, up to 755 K, on key pulse detonation engine performance parameters. This effort has identified certain limitations on detonation tube configuration, has provided an understanding of the pressure-temperature profile of the initial combustion event of the cycle, and for the first time has defined a measure of success rate for repetitive detonation cycles.

The effects of increasing fuel injection temperature on ignition time, DDT time, detonation distance, and detonation percentage for JP-8, JP-7, JP-10, JP-900, RP-1, and S-8 were determined. Ignition time was found to be virtually independent of fuel injection temperature for all fuels, except JP-8. JP-10 was found to produce undesirably low levels of detonations, compared to the other fuels. The DDT time of other five fuels demonstrated a nearly identical inverse relationship with fuel injection temperature; DDT time decreases linearly by approximately 15%. The detonation distance for all fuels, other than JP-10, linearly decreases with increasing fuel injection temperature. Above the flash vaporization temperature of the fuels, the detonation distance for all fuels is identical. The detonation percentage for all fuels increases considerably with increasing fuel injection temperature, with JP-7 and S-8 producing the most consistent detonations. Based on this performance criteria; JP-8, JP-7, JP-900, RP-1, and S-8 can all be used efficiently to fuel a PDE with elevated fuel injection temperatures.

The spark delay was found to have a small effect on all performance parameters for JP-8, although it was determined that operating the PDE with a spark delay below 4 msec yields very poor performance. A spark delay of 4 msec was found to be superior to the other spark delays studied for JP-8, based on total time to detonation and detonation percentage. The global reaction theory was shown to provide reasonable approximations for the effect of head pressure on ignition time. Increasing frequency was found to have a positive effect on the performance of a PDE. DDT time is inversely related to frequency, while ignition time and detonation distance are relatively independent of frequency.

Acknowledgments

This work would not have been possible without the technicians who worked on this project; our thanks to Curtis Rice, Dave Baker, and Dwight Fox (ISSI). Dr. Tim Edwards (AFRL/PRTG) was extremely helpful in developing the fuel systems for this work. The authors would also like to thank Jeff Stutrud (AFRL/PRTC) for his controls and data acquisition expertise and Capt. Wesley for his help. The technical leadership of Dr.

Robert Hancock (AFRL/PRTC) was invaluable. Funding was provided by the Air Force Research Laboratory, Propulsion Directorate and AFOSR.

References

[1]Miser, C. L., King, P. I., and Schauer, F. R. "PDE Flash Vaporization System for Hydrocarbon Fuel Using Thrust Tube Waste Heat," *41st AIAA/ASME/SAE/ASEE Joint Propulsion Conference and Exhibit,* Tucson AZ: AIAA 2005-3511, 10-13 July 2005.

[2]Tucker, K. C. "A Flash Vaporization System for Detonation of Hydrocarbon Fuels in a Pulse Detonation Engine," Ph.D. Dissertation, Department of Aeronautics and Astronautics, Air Force Institute of Technology, Wright-Patterson AFB, OH, 2005.

[3]Schauer, F. R., Stutrud, J. S., and Bradley, R. P. "Detonation Initiation Studies and Performance Results for Pulse Detonation Engine Applications," *39th AIAA Aerospace Sciences Meeting and Exhibit.* Reno NV: AIAA 2001-129, 8 - 11 January 2001.

[4]Tucker, K. C., King, P. I., Bradley, R. P., and Schauer, F. R. "The Use of a Flash Vaporization System with Liquid Hydrocarbon Fuels in a Pulse Detonation Engine," *42nd AIAA Aerospace Sciences Meeting and Exhibit.* Reno NV: AIAA 2004-0868, 5 - 8 January 2004.

[5]Helfrich, T. M. "Cycle Performance of a Pulse Detonation Engine with Supercritical Fuel Injection," M.S. Thesis, Department of Aeronautics and Astronautics, Air Force Institute of Technology, Wright-Patterson AFB, OH, 2006.

[6]Lefebvre, A., Freeman, W., and Cowell, L. "Spontaneous Ignition Delay Characteristics of Hydrocarbon Fuel/Air Mixtures," NASA CR-175064, 1986.

[7] Kaneshige, M. and Shepherd, J. E. *Detonation Database*. Technical Report FM97-8, GALCIT, July 1997.

[8]Shchelkin, K.L. "Soviet Journal of Technical Physics," Vol. 10, pg. 823-827, 1940.

[9]Spadaccini, L. J., Sobel, D. R., Haung, H., Dardas, Z., "Coke Deposition/Mitigation in Endothermic Fuels – Advanced Fuel Development and Fuel Combustion," AFRL-PR-WP-TR-1998-2098, June 1998.

[10]Bartok, W. and Sarofim, A. F. *Fossil Fuel Combustion – A Source Book.* New York City NY: John Wiley and Sons Incorporated, 1991.

[11]Miser, C. L., Helfrich, T. M., Schauer, F. R., and Phelps D. K. "Supercritical Fuel Density from Experimental Pulse Detonation Engine," *44th AIAA Aerospace Sciences Meeting*. Reno NV: AIAA 2006-1025. 9-12 January 2006.

[12]Panzenhagen, K. L. "Detonation Branching in a PDE with Liquid Hydrocarbon Fuel." M.S. Thesis, Department of Aeronautics and Astronautics, Air Force Institute of Technology, Wright-Patterson AFB OH, 2004.

[13]Miser, C. L. "Pulse Detonation Engine Thrust Tube Heat Exchanger for Flash Vaporization and Supercritical Heating of JP-8," M.S. Thesis, Department of Aeronautics and Astronautics, Air Force Institute of Technology, Wright-Patterson AFB OH, 2005.

[14]J. S. Zdenek and R. A. Anthenien, "Ion Based High-Temperature Pressure Sensor," *42nd AIAA Aerospace Sciences Meeting*, AIAA 2004-0470, Reno, NV, 2004.

[15]Coleman, Hugh W. and Steele, W. Glenn, Jr. *Experimentation and Uncertainty Analysis for Engineers*. New York NY: John Wiley and Sons Incorporated, 1989.

Performance Scaling of a Large Scale Unsteady-Driven Ejector System

Unsteady thrust augmentation was measured on a large scale driver/ejector system. A 72 in. long, 6.5 in. diameter, 100 lb_f pulsejet was tested with a series of cylindrical ejectors of varying length, and diameter. A tapered ejector configuration of varying length was also tested. The objectives of the testing were to determine the dimensions of the ejectors which maximize thrust augmentation, and to compare the dimensions and augmentation levels so obtained with those of other, similarly maximized, but smaller scale systems on which much of the recent unsteady ejector thrust augmentation studies have been performed. An augmentation level of 1.71 was achieved with the cylindrical ejector configuration and 1.81 with the tapered ejector configuration. These levels are consistent with, but slightly lower than the highest levels achieved with the smaller systems. The ejector diameter yielding maximum augmentation was an almost exact match to the small scale experiments, when scaled by the diameter of the driving jet. For this ejector, the length yielding maximum augmentation, when scaled by the diameter of the driving jet, was also the same as the small scale experiments. Testing procedures are described, as are the parametric variations in ejector geometry. Results are discussed in terms of their implications for general scaling of pulsed thrust ejector systems.

XI. Introduction

IN Recent years there has been renewed interest in the concept of ejectors or thrust augmentors driven by unsteady propulsion devices. The reason for this stems primarily from the interest in Pulse Detonation Engine (PDE) based propulsion systems, which are decidedly unsteady, and which therefore seem natural candidates on which to use an ejector. It has been suggested in the past[1], and shown convincingly in numerous recent experiments[2-9] that under the proper operating conditions, and with a well designed ejector, thrust augmentation levels approaching or even exceeding 2.0 can be achieved with unsteady thrust sources as drivers. Thrust augmentation is defined as the total time-averaged thrust provided by the ejector and driver system divided by the thrust of the driver alone.

$$\phi = \frac{\bar{F}_{total}}{\bar{F}_{driver}} \tag{1}$$

It has further been shown that these high levels can be reached using remarkably small ejectors in comparison to their steady state counterparts. Several studies have been conducted using actual PDE's as rivers[5, 7, 9]; however a number have used alternative unsteady thrust sources including simple pulsed valves, Hartmann resonance tubes, synthetic jets, and pulsejets[2-4, 6, 8]. The results from each of these varied experiments have helped identify the factors which contribute to the superiority of unsteady ejector systems in general (and therefore how they can be optimized), and which factors are unique to the particular driver. For example, it is now generally agreed that the frequency, unsteadiness level (the standard deviation of the exhaust velocity for example), and exhaust gas temperature of the thrust source play a significant role in the maximum thrust augmentation that can be achieved[6]. These and other parameters[10] characterize the emitted vortex associated with each pulse of any unsteady thrust device. This vortex plays a critical role in determining thrust augmentation, though the physical mechanism is not understood. It has been shown through experimental measurements for example that vortex diameter is closely matched to the diameter of the ejector yielding maximum thrust augmentation[5, 6, 10, 11]. On the other hand, it is believed that the strong emitted shock, uniquely associated with the PDE pulse, has a large, though currently not well understood, influence on the maximum attainable thrust augmentation.

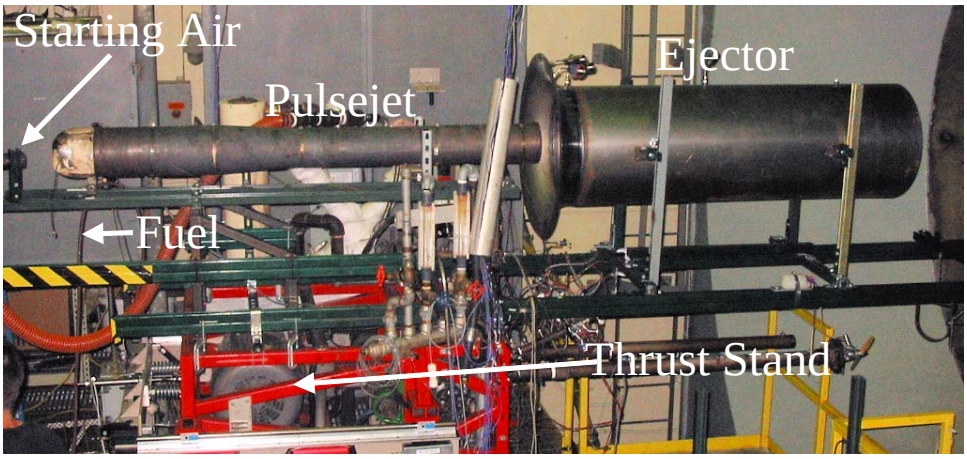

Figure 1. Experimental setup.

Despite the many unsteady ejector experiments performed to date, and the growing body of understanding associated with them, generalization of some results are not yet possible because the experiments have shared a common scale, which is to say small. The thrust levels have been low (less than 15 lb_f), and the physical dimensions of the thrust sources, in particular the driver diameters, have been between 1 and 2 inches. Rules have been suggested relating the optimal diameter of the ejector as a fixed ratio relative to that of the driver; however, they are not definitive because all the drivers tested are nearly the same size. The experiment described in this paper was developed to at least partially address this issue.

A large pulsejet, approximately an order of magnitude larger in exhaust cross-sectional area and thrust than most recent tests, was operated with a series of ejectors of varying cross section, length, and shape (cylindrical and tapered). The geometric ejector parameters, along with the spacing between the pulsejet tailpipe and ejector inlet were systematically varied in order to determine the configuration yielding the highest thrust augmentation, as measured by the thrust stand to which the system was mounted. The results were then compared to previous experiments both in terms of augmentation achieved and in terms of optimized ejector dimensions. This paper will describe the experiment including the major components (pulsejet, ejector sets, and thrust stand), construction, testing procedures, and parametric variations of ejector dimensions. Results will then be presented, and a discussion of findings will follow.

XII. Experimental Setup

The experimental setup is shown in Fig. 1 with the major components labeled. These are the ejector (1 of 4 tested), the pulsejet, and the thrust stand. Each will be described below.

G. Pulsejet Driver

The pulsejet tested and discussed in this paper is a Solar PJ32, originally developed and manufactured by the Solar Aircraft Company for the Globe Corporation Aircraft Division in 1951. Details of the device and performance characteristics are described in Ref. 13. Relevant dimensions are shown in the schematic of Fig. 2.

In brief, it is a self-aspirating, valved unit which operates on liquid fuel (Avgas in this experiment) that is fed directly into the combustion chamber via a pressurized fuel line. Like most pulsejets it requires forced air directed at the inlet and a high frequency sparking system in the combustion chamber in order to initiate operation. Once operation has commenced however, the resonant nature of the device does not require forced air or spark. The fact that that fuel supply is pressurized (as opposed to a venturi-based arrangement found in small scale units[3]) allows the pulsejet to be throttled in a reasonably predictable fashion. Figure 3 shows the relationship between measured thrust and fuel flow rate. Fuel flow rate is measured using an in-line turbine-type flow meter. Data is shown both from previous testing done to characterize the pulsejet[13], and from baseline testing done in the present experiment without an ejector installed. Also shown are a cubic fit to the data and the bounds representing two standard deviations above and below the fit. It can be seen that a certain amount of scatter is present, which appears to be typical for pulsejets. For the present experiment, the pulsejet was operated near the maximum thrust point during all testing. The scatter in this operating region results in a maximum uncertainty of ±7%. For the present baseline data shown the average absolute error between measured and curve-fit thrust was 3.7%. The maximum error was 6%

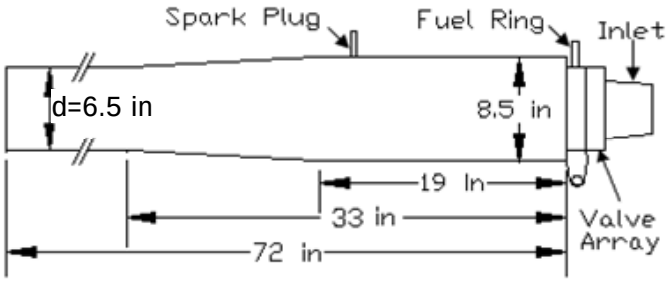

Figure 2. Pulsejet schematic.

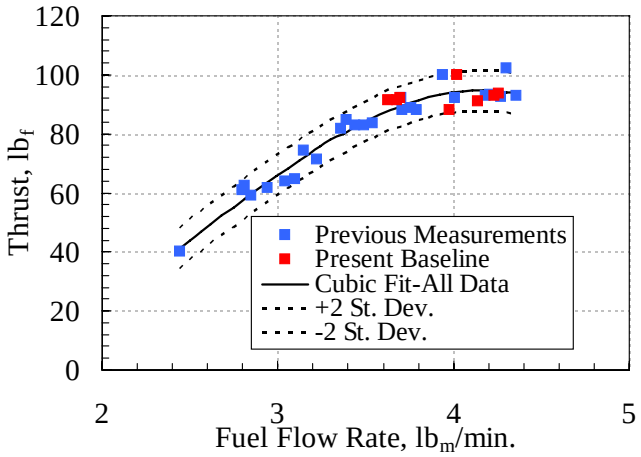

Figure 3. Pulsejet thrust as a function of fuel flow.

The thrust stand can only measure total system thrust (pulsejet and ejector combined); however, thrust augmentation can only be determined if the thrust of the jet alone is known. One way to determine this is to simply run the pulsejet on the thrust stand without an ejector and use that thrust value as the baseline for all subsequent ejector tests. However, it is prohibitively time consuming to do this for each of the many ejector configurations tested. As such, this measurement was made an average of once every sixteen operational runs of the engine. This method of determining jet-alone thrust will be referred to as Method I in subsequent sections of the paper where results are presented. If the rate of fuel flow could be accurately controlled, this method would suffice, save for the run-to-run uncertainty already described. The fuel flow rate through the system varied over time however, possibly due to clogging at the injectors. As such, the same pressure in the fuel system did not always yield precisely the same flow rate. To account for this, the jet-alone thrust was also determined using the curve-fit presented above and the measured fuel flow rate from each run. This measurement method, referred to later as Method II, could be made each run, with or without an ejector present.

The frequency of operation of this pulsejet was 69 hz., with a standard deviation of 2 hz. for all of the testing performed. The operational frequency is weakly, and inversely related to the fuel flow rate. The observed frequency of the present tests was, like the thrust values, consistent with that observed in previous tests. It is interesting to note in passing that the product of operational frequency and length on this pulsejet is 15% higher than that for the small scale unit used in Ref. 3. Pulsejets are often thought of as gas dynamic devices with a frequency that is determined by the end-to-end transit time of a fixed set of dominant waves. All other things being equal, this conception implies that the product of frequency and length should be a constant. The observed difference therefore either indicates that the average temperature of the combustion products is 30% higher in the large unit (which would probably melt the steel), or that there are other elements contributing to the resonance than simply wave reflections (e.g. Helmholtz-like behavior, heat release rate, etc.).

H. Ejectors

Four ejectors were constructed from mild-steel sheet ranging in gage from 18 to 20. Scaled drawings of each are shown in Fig. 4, which also shows symbolic nomenclature for the relevant dimensions. Those dimensions are listed in Table 1. The commercially available bellmouth inlets were seamless, and terminated with a 1.0 in. long straight section. The main body of each cylindrical ejector was composed of a single rolled piece with a welded seam along the length. It was joined to the bellmouth with a circumferential weld. The main body of the tapered ejector was composed of two symmetric halves. The conical shape was achieved through a process called "bumping" whereby a small bend is applied approximately every inch along the circumference. This actually creates a many-sided polygon rather than a pure circular cross-section. The two halves were welded together along the entire length. The finished body was then attached to the inlet with a circumferential weld.

The dimensions of the ejectors were chosen by a geometrical scaling of the small scale ejectors tested in the pulsejet-based experiments of Ref. 3. The length and diameter of the Ref. 3 ejector yielding the highest thrust augmentation was normalized by the diameter of the pulsejet driver (1.25 in.). Those ratios were then multiplied by the pulsejet diameter in the present work (6.5 in.) to obtain the length and diameter of the central ejector. The other two diameters were then selected as 20% smaller and 25% larger than the central value with the supposition that this span would be sufficient to bound value of the optimal diameter. The inlet radius, R was not variable because the bell mouth inlets were commercially available, stock-items, and the radius was pre-determined based on the diameter, D selected. It has been shown however that, while inlet rounding is necessary (a sharp-edged inlet will produced almost no augmentation), rounding beyond values of R/D=0.15 shows little benefit. The ejectors used in this experiment had R/D≥0.20.

Table 1 Ejector dimensions (as-built)

R (in.)	L (in.)	D (in.)
Straight, cylindrical		
3	64	13
4	65	16
4	65	20
Tapered, conical		
4	70	16

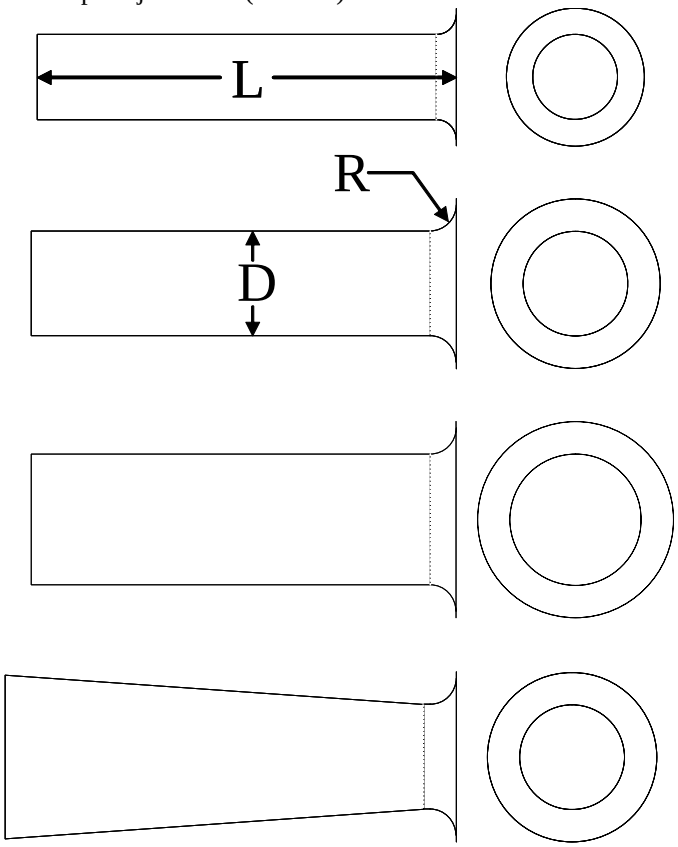

Figure 4. Ejector schematics and symbols for relevant dimensions.

I. Thrust Stand

Details of the thrust stand have been presented elsewhere in the literature[9, 14]. As such only a brief description will be given here. It consists of a cart with linear bearings which ride along a pair of fixed, low-friction rails. The test article (pulsejet or pulsejet and ejector combination) is rigidly attached to the cart. The cart pushes against a damped, calibrated spring, one end of which is fixed. Thrust is ultimately determined by measuring the cart displacement with a positional sensor which is low-pass filtered with a cut-off frequency of 0.5 hz. A time trace of measured thrust during a typical test run is shown in Fig. 5. The damping and filtering system is evidently quite effective, as there are no oscillations in the measured thrust. It is noted that there is a small positive thrust measured prior to engine ignition. This is the result of stiction in the damping system. During operation, stiction is overcome by the impulsive delivery of thrust.

J. Test Procedure

Each test run was approximately 30 seconds in duration and consisted of the following sequence. Fuel pressure was set. Starting air was then turned on. Shortly thereafter the fuel flow valve was opened, with a near simultaneous activation of the spark. Shortly after engine operation commenced, the starting air and spark were shut off. After approximately 15 seconds, the thrust reading would level off and for the next 15 seconds thrust was measured at approximately 1.0 second intervals. After the thrust measurement was acquired the fuel valve was closed, and the starting air was re-activated in order to provide cooling. The thrust data to be presented represents a simple time-average over the 15 second sampling period. This basic sequence is illustrated in Fig. 5 which shows actual test data from a typical run.

For each ejector tested the baseline thrust of the pulsejet was first measured without the ejector present. A straight-sided ejector was then mounted on the thrust stand, with its axis of symmetry aligned with that of the pulsejet. Thrust measurements were made with the ejector inlet placed at various axial positions relative to the exhaust plane, as shown in Fig. 6. For each ejector, an optimal spacing value was found which yielded the highest thrust augmentation. This procedure was followed for each of the three straight ejector diameters.

The diameter yielding the highest thrust augmentation was then selected for length variation testing. It was first lengthened by welding a 19.5 in. extension to the cylindrical section, at the exhaust end. This modified ejector was then tested according to the procedure just described. The length of the ejector was then reduced by simply cutting off a portion of the exhaust end. The length reduction was done in increments of one pulsejet diameter (6.5 in.).

Due to time limitations, only one tapered ejector was tested. The minimum diameter of this ejector was chosen to be the same as that of the cylindrical ejector yielding the highest thrust augmentation. A tapered ejector made the same way was tested on several small scale rigs and found to yield very high thrust augmentation levels[1, 5, 15]. The spacing and length of this ejector were varied in the manner described above; however, no extension was made to the initial 70 in. length.

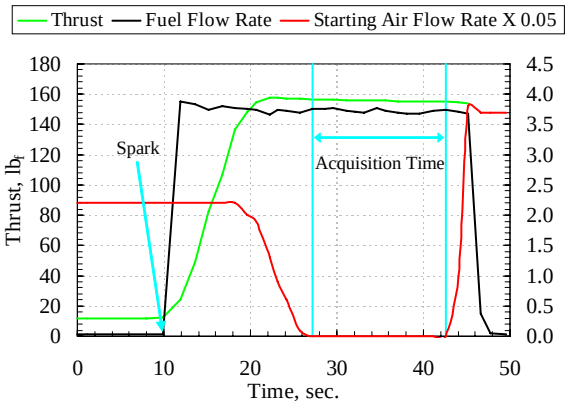

Figure 5. Measured thrust as a function of time for a typical pulsejet and ejector combination. Fuel and starting air flow rates are also shown.

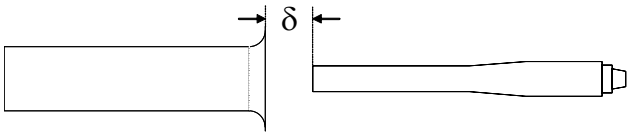

Figure 6. Schematic of ejector spacing variation. The schematic is to scale.

XIII. Results and Discussion

K. Straight, Cylindrical Ejectors

1. Driver-to-Ejector Spacing Variations

Although spacing variation testing was performed on every ejector configuration, the results tended to be similar in trend. As such, results from only one configuration will be shown. Fig. 7 displays the thrust augmentation as a function of driver-to-ejector spacing for the 16 in. diameter ejector, of 65 in. length. The spacing has been normalized by the driver diameter, *d*. Results are presented using both Methods I (baseline measured pulsejet thrust) and II (pulsejet thrust estimated from the fuel flow curve-fit of Fig. 3) to compute thrust augmentation. Also shown are the results from the small scale pulsejet experiment of Ref. 3. Negative values of ejector spacing indicate that the exhaust plane of the pulsejet was actually inside the ejector. In the Ref. 3 experiment, such measurements were not possible as the pulsejet would cease to operate at low spacing values. The same phenomenon occurred in the present experiment, but at much smaller, even negative values. It is interesting to note that the augmentation reaches a peak as the ejector and driver are brought closer together. It then decreases to a minimum, and begins to rise again as the driver is brought into the ejector

interior. It is not known whether a second peak exists because, as mentioned, the pulsejet stopped operating. Such 'twin peak' behavior was observed in the PDE driven experiment of Ref. 5. The spacing yielding peak performance is approximately 2.0 pulsejet diameters. This value is similar to, but slightly larger than, the value found in the small scale experiment. Comparison with other experimental results[4,5] indicates that the value varies between 1 and 2.5 driver diameters. It therefore appears to be a somewhat experiment specific parameter, perhaps depending on both the physical geometry of the driver and the characteristic of the unsteady pulse.

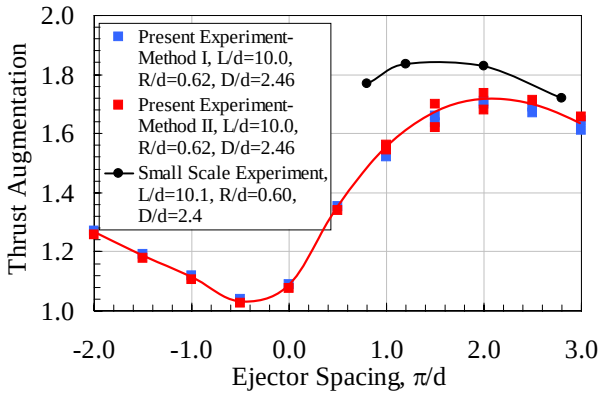

Figure 7. Thrust augmentation as a function of driver-to-ejector spacing for the D/d=2.46, L/d=10.0 ejector.

Optimal ejector spacing was found to be invariant with changing ejector length. However, it should be kept in mind that only one diameter ejector was varied in this manner.

For variations in diameter using a fixed length, the optimal spacing followed a nearly perfect linear relationship described by

$$\left(\frac{\delta}{d}\right)_{optimal} = 0.901\left(\frac{D}{d}\right) - 0.271 \qquad (2)$$

The general increase in optimal spacing as ejector diameter increases is consistent with the results of Refs. 3-5.

2. EjectorDiameterVariations

Thrust augmentation levels obtained with optimally spaced, fixed length ejectors are shown as a function of ejector diameter in Fig. 8. The ejector diameter has been normalized by the driver diameter. Once again, results using both Methods I and II to obtain pulsejet thrust are shown. For comparison, results from the small scale pulsejet experiment also appear. There is a clear optimal ejector diameter, and for both the large and small scale experimental results it appears to be very nearly 2.5 driver diameters. This result is remarkably consistent over a range of drivers. Table 2 lists the ejector to driver diameter ratios at which peak augmentation levels were found in a number of experiments using cylindrical or nearly cylindrical ejectors. The values all fall between 2.4 and 3.0, indicating that the optimal ejector diameter is a near constant multiple of the driver diameter, probably having a weaker secondary dependence on other, as yet unknown parameters. This result supports the notion the vortex emitted with each pulse of the driver plays a key role in unsteady thrust augmentation since, as was pointed out in Refs. 5 and 6, its size (bounding diameter) appears to follow

Table 2 Optimal D/d values.

Ref.	Driver Type	ϕ_{max}	Optimal D/d	d (in.)
Present	Large Pulsejet	1.71	2.4	6.50
2	Chopped Pulse	1.45	3.0	3.14
3	Small Pulsejet	1.83	2.5	1.25
4	Resonance Tube	1.38	2.7*	1.50
5	PDE	2.00	3.0	1.00
6	Synthetic Jet	1.67	2.4+	0.93
7	PDE	2.10	3.0	1.93

* Using the hydraulic diameter of the driver 275 hz. driver.
+ Using 'effective diameter' measured w/ PIV.

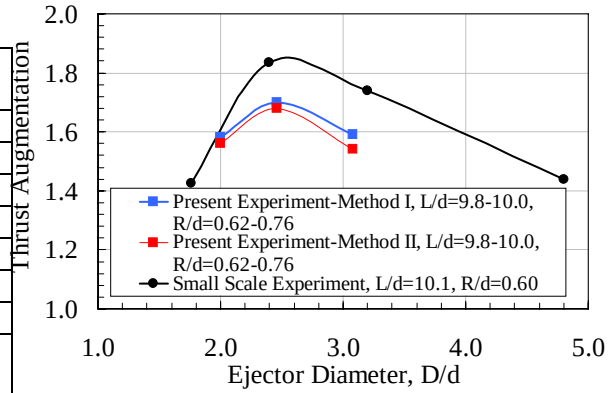

Figure 8. Thrust augmentation as a function of ejector diameter for the L/d=10.0 ejectors. The ejectors are optimally spaced for each point.

the same ratio when divided by the driver diameter.

It is noted that although the value of D/d is nearly the same for all of these ejectors, the thrust augmentation obtained is not. Part of the reason for this may be that while all of the unsteady drivers emit a vortex, the amount of vorticity present, the balance between fluid trapped in the vortex and that which follows behind, and the interaction between vortex bound fluid and trailing jet fluid may be vastly different. These features may play a key role in the entrainment of and momentum transfer to the secondary fluid in the ejector, although the mechanism isn't clear [6, 16].

It was suggested in Ref. 6 that a characterizing feature of the emitted vortex, the Formation Number[17] may be a correlating parameter to the peak thrust augmentation achievable with an ejector that has been optimized for length and diameter. In that paper, the formation number was defined as

$$F = \frac{\sqrt{\overline{u'^2}}}{2fd} \tag{3}$$

where f is the frequency of operation, and $\sqrt{\overline{u'^2}}$ is the root mean square of the periodic velocity fluctuations in the exit plane of the driver. This velocity can be estimate from measured thrust, mean flow rate and temperature of the driving jet. It was argued that peak thrust augmentation should rise with Formation Number up to some critical value, F_{crit}. Beyond this number, peak thrust augmentation should slowly fall. Figure 9 shows the peak thrust augmentation obtained as a function of Formation Number for the present experiment and several others for which sufficient data was available[‡]. A simple parabolic fit through the data is also shown. The data seems to follow the expected trend, indicating a value of F_{crit} near 40; however, the data is admittedly sparse and much more is needed. Furthermore, it was noted in Ref. 6 that other factors such as the exhaust gas temperature (relative to the entrained secondary flow) may play a significant role in determining peak thrust augmentation. The experiments represented in Fig. 9 have vastly different exhaust temperatures for which no accounting has been made other than the effect on $\sqrt{\overline{u'^2}}$. Beyond this, the use of Formation Number as is done here provides no insight into the physical mechanism of unsteady thrust augmentation. It only provides a potentially predictive correlating parameter, albeit one that is fairly compelling.

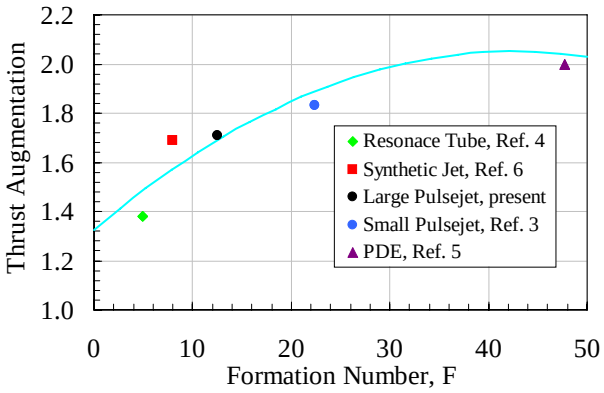

Figure 9. Peak thrust augmentation as a function of Formation Number for the present and several other experiments.

3. Ejector Length Variation

As stated earlier, length variation tests were only performed on a single cylindrical ejector. The 16 in. diameter ejector was chosen (D/d=2.46) diameter ejector since it had yielded the highest performance at the as-built 65 in. length. The variation in thrust augmentation as a function of ejector length is shown in Fig. 10. The length has been normalized by the driver diameter. Results from the small pulsejet experiment of Ref. 3 are also shown. The trends of the two experiments are somewhat different; however, it is noted that the peak value of thrust augmentation occurs at the same value of L/d=10 for both. This turned out to be the as-built length in the present experiment.

This ratio does not hold for the other unsteady experiments; however, it is not clear that it should. There are several conceptual models for the mechanism by which fluid is entrained and energized in the ejector. One posits a sort of piston-like behavior of the driver flow which delivers momentum to the secondary flow via

[‡] For the Ref. 5 PDE experiment the rms velocity was obtained from a numerical simulation matching flow rate and thrust. Because the exhaust flow is highly impulsive, only the thrust producing period was used in the rms velocity calculation. The inverse of this period was used for f in Eqn. 3

direct pressure exchange as the two flows collides within the ejector. A second notion suggests that the mechanism of entrainment and momentum exchange is the same as that for a steady ejector, namely shear flow and mixing (most likely driven by turbulence). Secondary fluid is literally dragged into the ejector and accelerated. In this conception, the emitted vortex serves the function of vastly increasing the shearing surface area (compared to a steady jet) due both to its initial structure and to its observed disintegration[§].

If the latter mechanism is correct, it might be expected that the emitted vortex would decelerate (even as it broke apart) at a rate proportional to its surface area and to the square of the difference between its velocity and that of the secondary flow. That is

$$U_v \frac{dU_v}{dx} \approx -\alpha\left(\frac{\rho_s}{\rho_v}\right)\left(\frac{S}{V}\right)(U_v - U_s)\text{^}2 \tag{4}$$

where ρ_v is the density of the vortex, *V* is the vortex volume, S is the surface area, U_v is the velocity of the vortex U_s is the average velocity of the secondary flow v, α is a constant, and ρ_s is the density of the secondary flow. Assuming that the vortex volume and surface area are proportional to the cube and square of its diameter respectively, and assuming further that its diameter is proportional to the diameter of the driver, the ratio (S/V) in Eqn. 4 simply becomes proportional to (1/d), i.e.

$$U_v \frac{d(U_v - U_s)}{d(x/d)} \approx -\kappa\left(\frac{\rho_s}{\rho_v}\right)(U_v - U_s)\text{^}2 \tag{5}$$

With κ a constant, Eqn. 5 can be solved numerically to yield *x/d* as a function of (U_v-U_s), for any given ρ_s/ρ_v and $U_v^{initial}/U_s$, which is the initial vortex velocity as it enters the ejector divided by the average secondary flow velocity. If the optimal ejector length, L_{opt} is defined as that value of *x* for which (U_v/U_s-1) is less than some specified small value such as 0.1, and if estimates of $U_v^{initial}/U_s$ and ρ_s/ρ_v are available, then Eqn. 5 can be used to obtain L_{opt}/d. This is illustrated in Fig. 11 which shows the numerical solution to Eqn. 5 for different values of the parameters $U_v^{initial}/U_s$ and ρ_s/ρ_v.

Estimates for $U_v^{initial}$ and U_s were obtained for the Refs. 3, 4, and 5 experiments using PIV data from Refs.

Table 3 Vortex and secondary flow velocities, and optimal L/d values.

Ref.	Driver Type	U_v (ft/s)	U_s (ft/s)	$\frac{\rho_s}{\rho_d}$	L_{opt}/d
3	Small Pulsejet	460	303	3.0	10.1
4	Resonance Tube	275	245	1.0	6.5
5	PDE	800	115	3.0	14.6

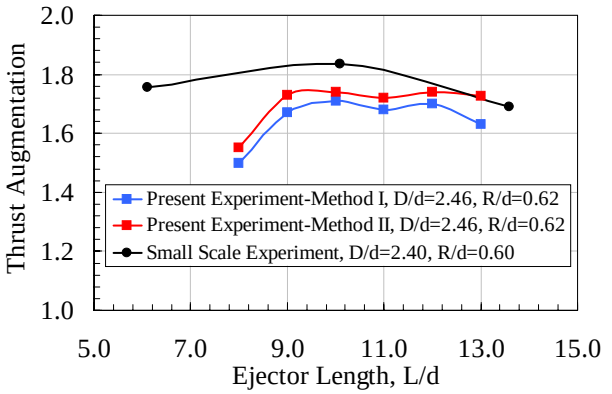

Figure 10. Thrust augmentation as a function of ejector length for the D/d=2.46 ejector. The ejectors are optimally spaced for each point.

[§] Observation of vorticity in the ejector exit region of the Refs. 11 and 12 indicate no coherent vortical flow structure at radial distances less than the ejector diameter.

Table 4 Optimal ejector and actual driver operational frequencies.

Ref.	Driver Type	f_{opt} (hz.)	f_{driver} (hz.)
3	Small Pulsejet	350	220
4	Resonance Tube	335	275
5	PDE	135	20

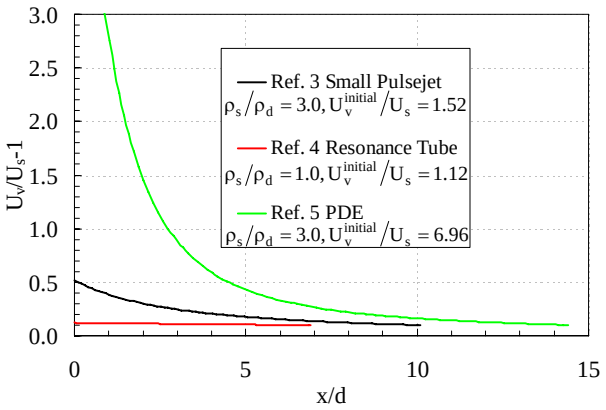

Figure 11. Numerical solution to Eqn. 5 for several relevant parameters of density ratio and vortex velocity ratio.

6, 11, and 12[**]. They are listed in Table 3. Values of ρ_s/ρ_v were not available. For the Ref. 4 resonance tube, this ratio should be near 1.0 since the driver gas was at near ambient temperature. For the Refs. 3 and 5 pulsejet and PDE driven experiments the ratio was estimated at approximately 3.0. This estimate assumes that the very hot, low density gas from each driver entrains a certain amount of cooler air as it forms the emitted vortex.

When these values of $U_v^{initial}$, U_s, and ρ_s/ρ_v were used in the numerical solution of Eqn. 5, together with a value of κ=0.32, and the ending criteria (U_v/U_s-1) =0.1, it was found that the values for L_{opt}/d obtained were almost exactly the values found experimentally, and listed in Table 3. This result is by no means proof of the shear mechanism for ejector entrainment and thrust augmentation, particularly given the scarcity of data and the density estimates used. It is nevertheless suggestive that this mechanism predominates.

It is interesting to note that Eqn. 5 may be rewritten as an ordinary differential equation in time as

$$\frac{d(U_v - U_s)}{dt} \approx -\frac{\kappa}{d}\left(\frac{\rho_s}{\rho_v}\right)(U_v - U_s)\text{^}2 \qquad (6)$$

Integrating this equation using the parameters listed above presumably gives the time required for the emitted vortex to travel down the ejector, decelerate, degenerate, and accelerate the secondary fluid. The inverse of this time provides an estimate for the optimal operational frequency from the perspective of shear-driven momentum transfer. For the Refs. 3, 4, and 5 experiments, these frequencies are listed in Table 4, along with the actual operational frequencies of the devices. All other things being equal, it would be intuitively expected that the closer together the optimal and operational frequencies, the higher the thrust augmentation. If this is true, it suggests that PDE's which for a given length ideally operate at much higher frequencies than that listed in Table 3, could obtain even higher augmentations levels than have been reported to date. It would also suggest that the present experiment, while generally exhibiting lower overall thrust augmentation values compared to those of the small scale pulsejet experiment of Ref. 3., is better matched in terms of this criteria. The value of L_{opt}/d found in the present experiment is identical to that of Ref. 3. It is expected that the values of ρ_s/ρ_v, $U_v^{initial}$, U_s are therefore quite similar. These can be used to integrate Eqn. 6 but with the larger diameter of the present experiment. The optimal frequency is found to be 67 hz., which is very close to the actual operating frequency of 69 hz.

L. Tapered, Conical Ejector

[**] For the Ref. 4 experiment, U_s was otained from unpublished hotwire measurements taken in the exit plane of the ejector.

As mentioned only one diameter of tapered, conical ejector was tested. The length was varied using the same technique that for the cylindrical ejector. Similarly, at each length the driver-to-ejector spacing was varied until the highest augmentation was achieved. As with the straight ejectors, this optimal spacing was very nearly 2 driver diameters for every length. The results of the length variation tests are shown in Fig. 12, along with those from the small scale pulsejet experiment of Ref. 3. Like the small scale experiment, the maximum augmentation achieved was higher with the tapered ejector than with the best of the straight type. Both experiments also show much more sensitivity at the shorter lengths than was seen with the straight ejectors. However, the small scale experiment has a clear length at which peak augmentation is observed, whereas the present experiment exhibits nearly flat region where the augmentation high and insensitive to length. The start of this region and the peak performance point of the small experiment both appear to occur between $8<L_{opt}/d<8.5$. The peak augmentation obtained in the present experiment was 1.83, while the small scale experiment yielded a value of 1.98. The same trend was seen with the straight ejectors. As mentioned earlier, part of the reason for this may be the due to the somewhat different vortex parameters associated with the two drivers (despite their both being valved pulsejets). Some of the difference may be attributed to the slightly different nature of the ejectors used in the two experiments, though these are fairly subtle. Figure 13 shows a cross section of the best performing straight and tapered ejectors used in the Ref. 3 work. The straight ejector is seen to actually have a short diffusing section at the exhaust end, and both have a half circle inlet profile as opposed to the quarter round profile of the present work.

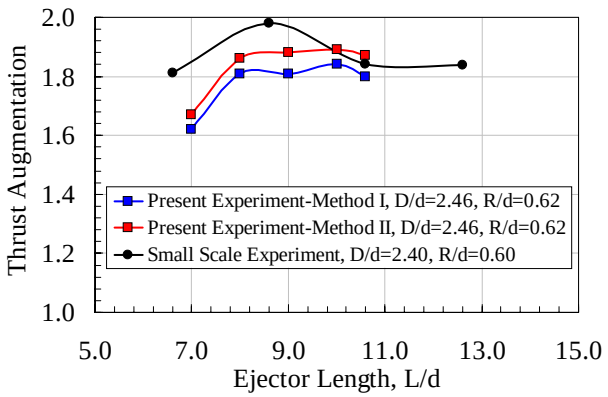

Figure 12. Thrust augmentation as a function of ejector length for the D/d=2.46 tapered ejectors. The ejectors are optimally spaced for each point.

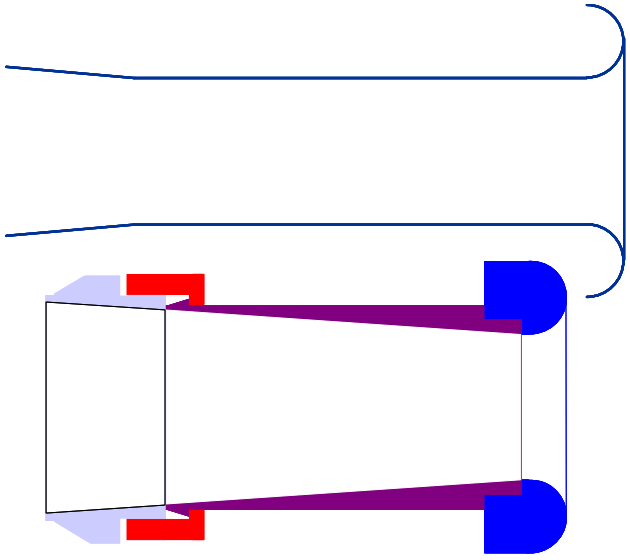

Figure 13. Straight and tapered ejector profiles used in the small scale pulsejet experiment of Ref. 3.

Another possible explanation for the comparatively lower peak augmentation in the large system may lie in the scale of the turbulence which is involved in the exchange of momentum between the driver and the secondary flow. There are numerous potential turbulence length scales in a pulsejet. Some are governed by the physical size of the unit, but others are not. It is possible that the scales from say, combustion, and the exhaust plane shear layer coincide in the small unit and thus, being encased in the emitted vortex, efficiently transfer the large scale vortex rotational energy to the secondary flow. In the large unit, this matching of scales may not hold. Of course, there is no proof yet for this (rather vague) explanation other than the observation that the measured turbulence levels in the emitted vortex of several unsteady thrust experiments are quite high[6, 11, 12]. Clearly, much more investigation is needed into the issue of peak thrust augmentation in unsteady thrust systems in general, and in large versus small systems in particular.

XIV. Conclusion

A large scale pulsejet-driven ejector system was tested with the objective of obtaining ejector dimensions which maximize thrust augmentation. Tests were conducted using ejectors of various length, diameter, and cross sectional profile. The spacing between the pulsejet exit and ejector inlet was also examined for its influence on performance. Comparisons with other unsteady ejector experiments were also made both in the level of augmentation achieved and in the dimensions of the optimized ejectors. A peak thrust augmentation value of 1.71 was obtained with straight ejectors. The optimized ejector diameter was found to be 2.46 times the pulsejet driver diameter of 6.5 in. This ratio was observed to be nearly constant over numerous experiments and may therefore be a sizing rule. The optimal length was found to be 10 time the driver diameter. This result was found to be the same as another, small scale pulsejet experiment, but different from those where another driving source was used. It was found that the tapered profile ejector yielded higher thrust augmentation value than the best from the straight profile series. The value obtained was 1.81. This result was consistent with numerous other unsteady thrust augmentation experiments. No variation in taper angle was performed and the optimal value remains unknown.

References

[1]Lockwood, R. M. "Interim Summary Report on Investigation of the Process of Energy Transfer from an Intermittent Jet to Secondary Fluid in an Ejector-Type Thrust Augmenter," Hiller Aircraft Report No. ARD-286, March, 1961.

[2]Binder, G. and Didelle, H, "Improvement of Ejector Thrust Augmentation by pulsating or flapping Jets," Paper E3 of Proc. 2nd Symposium on Jet Pumps & Ejectors and Gas Lift Techniques, Cambridge, England, March 1975.

[3]Paxson, D. E., Wilson, J., and Dougherty, K. T., "Unsteady Ejector Performance: An Experimental Investigation Using a Pulsejet Driver," AIAA paper 2002-3915, July, 2002.

[4]Wilson, J., and Paxson, D. E., "Unsteady Ejector Performance: An Experimental Investigation Using a Resonance Tube Driver," AIAA paper 2002-3632, July, 2002.

[5]Wilson, J., Sgondea, A., Paxson, D. E., Rosenthal, R., "Parametric Investigation of Thrust Augmentation by Ejectors on a Pulsed Detonation Tube," AIAA paper 2005-4208, July, 2005.

[6]Paxson, D. E. Wernet, M. P., John, W. T., "An Experimental Investigation of Unsteady Thrust Augmentation Using a Speaker-Driven Jet," AIAA 2004-0092, January, 2004.

[7]Landry, K., Shehadeh, R., Bouvet, N., Lee, S.-Y, Pal, S., and Santoro, R. J., "Effect of Operating Frequency on PDE Driven Ejector Thrust Performance," AIAA paper 2005-3832, July, 2005.

[8]Choutapalli, I. M., Alkislar, M. B., Krothapalli, A. Lourenco, L. M., "An Experimental Study of Pulsed Jet Ejector," AIAA paper 2005-1208, January, 2005.

[9]Allgood, D. Gutmark, E. Hoke, J. Bradley, R., Schauer, F., "Performance Measurements of Pulse Detonation Engine Ejectors," AIAA paper 2005-223, January, 2005.

[10]Wilson, J. "Effect of Pulse Length and Ejector Radius on Unsteady Ejector Performance," AIAA paper 2005-3829, July, 2005.

[11]John, W. T., Paxson, D. E., Wernet, M. P., "Conditionally Sampled Pulsejet Driven Ejector Flow Field Using DPIV," AIAA paper 2002-3231, June, 2002.

[12]Opalski, A. B., Paxson, D. E., Wernet, M. P., "Detonation Driven Ejector Exhaust Flow Characterization Using Planar DPIV," AIAA paper 2005-4379, July, 2005.

[13] Litke, P. J., Schauer, F. R., Paxson, D. E., Bradley, R. P., Hoke, J. L., "Assessment of the Performance of a Pulsejet and Comparison with a Pulsed-Detonation Engine," AIAA paper 2005-0228, January, 2005.

[14]Schauer, F. R., Stutrud, J., and Bradley, R. P., "Detonation Initiation Studies and Performance Results for Pulsed Detonation Engine Applications," AIAA Paper 2001-1129, January 2001.

[15]Paxson, D. E., "2003 Pulse Detonation Engine Project: University/Government Spring Ejector Meeting," unpublished presentation, 2003.

[16]Wilson, J. "Vortex Rings Generated by a Shrouded Hartmann-Sprenger Tube," AIAA paper 2005-5163, June 2005.

[17]Gharib, M., Rambod, E., Shariff, K., "A universal time scale for vortex ring formation," *Journal of Fluid Mechanics*, Vol. 360, pp. 121-140, 1998.